IMPACT: A Parallel Multi-Physics Beam Dynamics Simulation Package

Ji Qiang

Accelerator Modeling Program

BLAST Workshop, May 7-9, 2018, Berkeley

BERKELEY LAB

U.S. DEPARTMENT OF ENERGY | Office of Science

ACCELERATOR TECHNOLOGY & APPLIED PHYSICS DIVISION ATAP

IMPACT: Integrated Map and PArticle TraCking

- The IMPACT(-Z depend.) started around middle of 90s (R. Ryne) including:
  - Drift, Quadrupole, RF linear transfer map
  - one 3D space-charge solver with open BCs
  - a few thousand lines of High Performance Fortran (HPF) code
- Redesign of the IMPACT code around the end of 90s (J. Qiang):
  - object-oriented design and implementation using F90
  - domain decomposition parallelization using MPI
  - multiple 3D space-charge solvers with open BCs, periodic BCs, conducting pipes

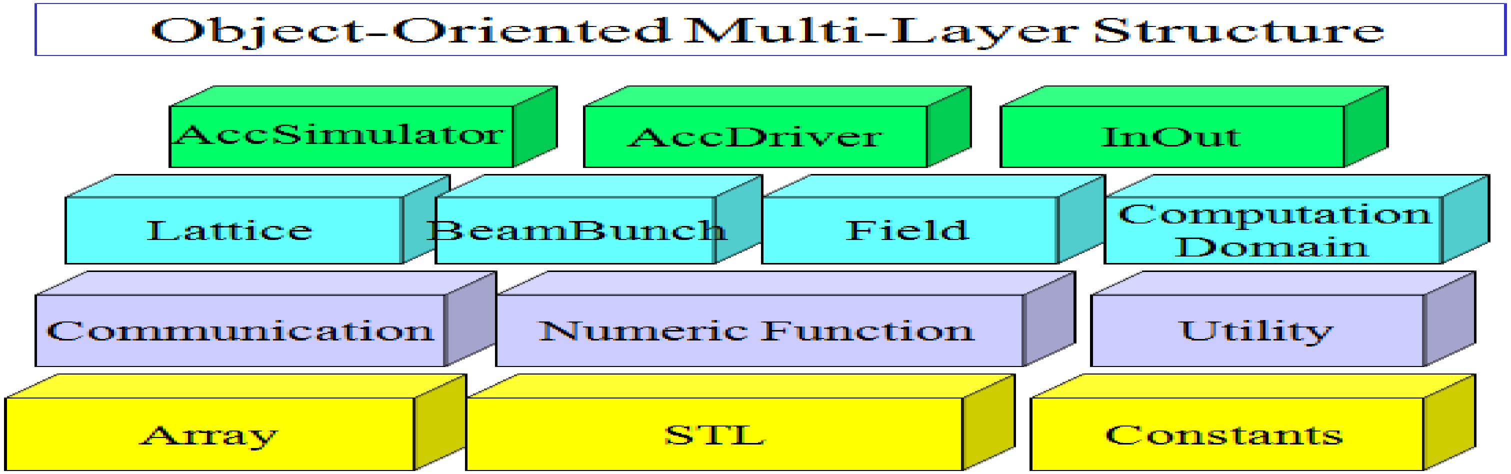

IMPACT: Recent Advances

- Current Features (with >100,000 lines of code) include:
  - Z dependent and T dependent tracking
  - Detailed 3D RF accelerating and focusing model, dipole, solenoid, multipole, ...
  - Multiple charge states, multiple bunches
  - 3D shifted-integrated Green's function space-solver
  - 3D spectral finite difference multigrid space-solver
  - Structure + resistive wall wakefields
  - CSR/ISR
  - Gas ionization
  - Photo-electron emssion
  - Machine errors and steering
- Can be used to model beam dynamics in:
  - Photoinjectors
  - Ion beam formation and extraction
  - RF linacs
  - Rings

Governing Equations in the IMPACT Code

$$\frac{\partial f(\vec{r},\vec{p},t)}{\partial t}+\dot{\vec{r}}\frac{\partial f(\vec{r},\vec{p},t)}{\partial \vec{r}}+\dot{\vec{p}}\frac{\partial f(\vec{r},\vec{p},t)}{\partial \vec{p}}=0$$

$$\dot{\vec{r}}=\frac{\partial H}{\partial \vec{p}}$$

$$\dot{\vec{p}}=-\frac{\partial H}{\partial \vec{r}}$$

$$H \doteq H_{ext}+H_{sc}$$

$$\nabla^2\phi=-\rho/\varepsilon \qquad \rho=\iiint f(r,p,t)d^3p$$

One Step Particle-In-Cell Method

$$f(\vec{r},\vec{p},t)=\sum\delta(\vec{r}-\vec{r}_p)\delta(\vec{p}-\vec{p}_p)$$

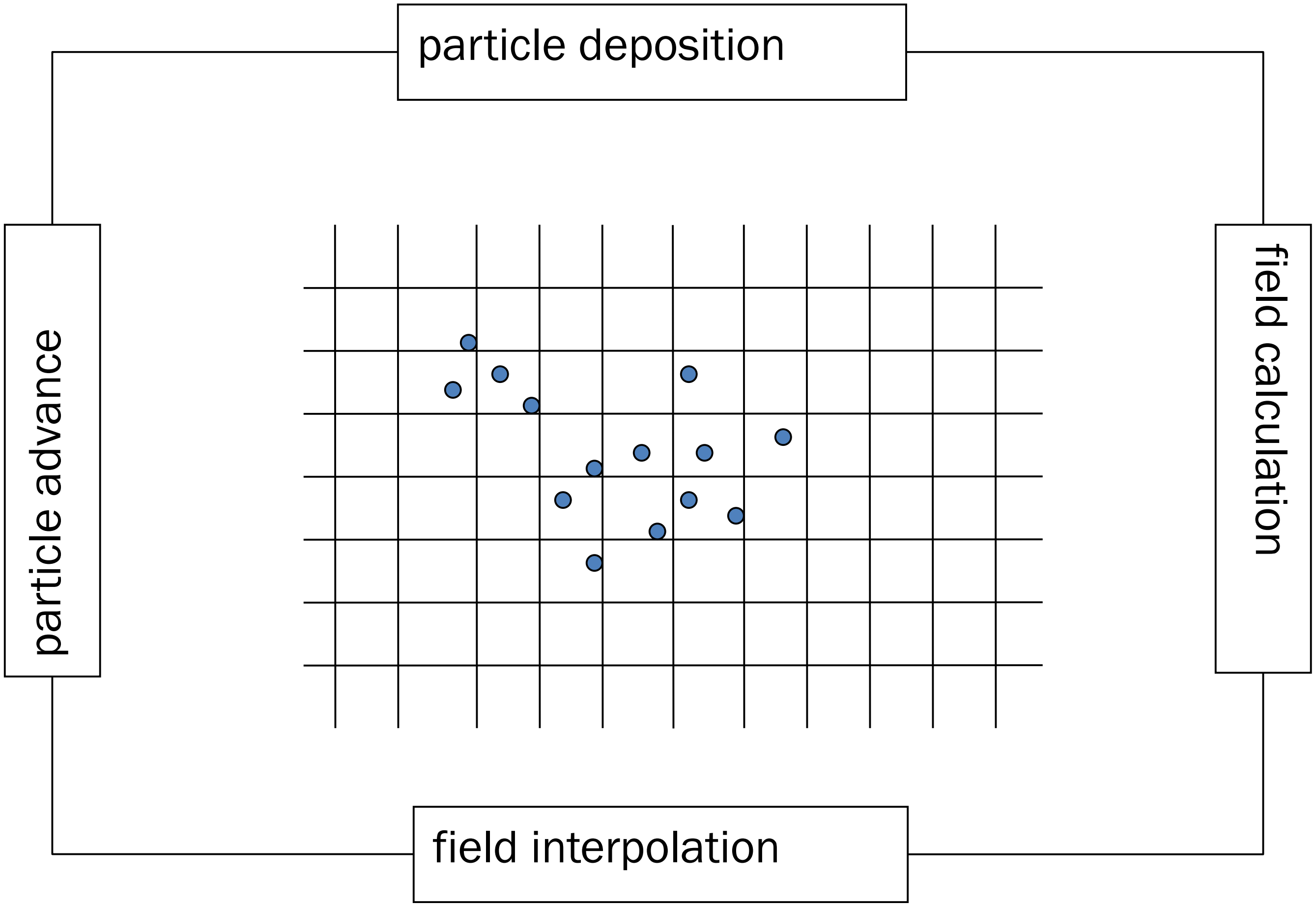

Split-Operator Method for Particle Advance

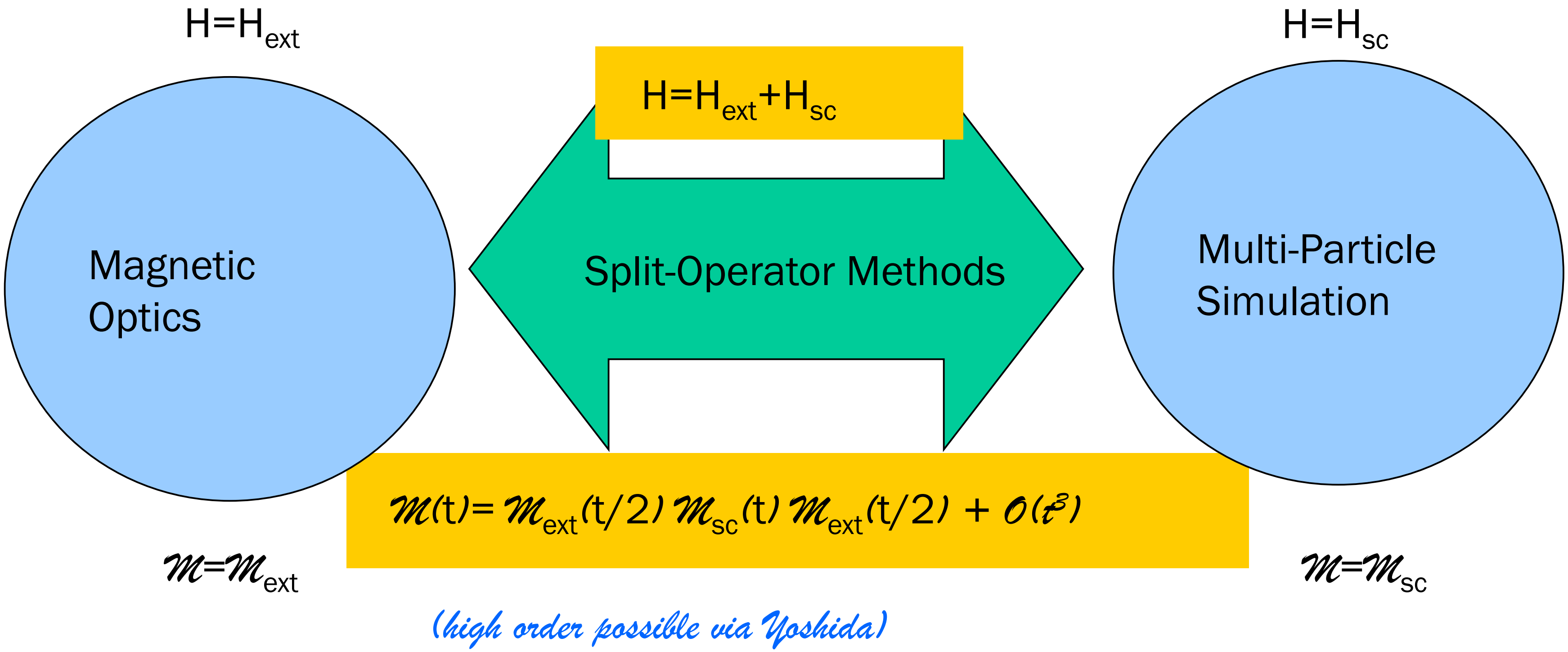

- Rapidly varying s-dependence of external fields is decoupled from slowly varying space charge fields
- Leads to very efficient particle advance:
  - Do not take tiny steps to push millions - billions of particles
  - Do take tiny steps to compute maps; then push particles w/ maps

Different Boundary/Beam Conditions Need Different Efficient Numerical Algorithms O(Nlog(N)) or O(N)

FFT based Green function method:

- Standard Green function: low aspect ratio beam
- Shifted Green function: separated particle and field domain
- Integrated Green function: large aspect ratio beam
- Non-uniform grid Green function: 2D radial non-uniform beam

Fully open boundary conditions

Spectral-finite difference method:

2D open boundary
Transverse regular pipe with longitudinal open

Multigrid spectral-finite difference method:

Transverse irregular pipe

J. Qiang, S. Paret, "Poisson solvers for self-consistent multiparticle simulations," ICFA Mini-Workshop on Beam-Beam Effects in Hadron Colliders, March 18-22, 2013.

Green Function Solution of Poisson's Equation (I)
(open boundary conditions)

$$\phi(r) = \int G(r, r')\rho(r')dr' \qquad ; \; r = (x, y, z)$$

$$\phi(r_i) = h \sum_{i'=1}^{N} G(r_i - r_{i'})\rho(r_{i'})$$

$$\boxed{G(x, y, z) = 1/\sqrt{(x^2 + y^2 + z^2)}}$$

Direct summation of the convolution scales as N^2 !!!!

N – total number of grid points

FFT based Hockney's Algorithm /zero padding:- *scales as (2N)log(2N)*

- Ref: Hockney and Easwood, ***Computer Simulation using Particles***, McGraw-Hill Book Company, New York, 1985.

$$\phi_c(r_i) = h \sum_{i'=1}^{2N} G_c(r_i - r_{i'})\rho_c(r_{i'})$$

$$\phi(r_i) = \phi_c(r_i) \quad \text{for i} \; = \; 1, \text{N}$$

Integrated Green Function Method (II)
(large aspect ratio beam with open boundary conditions)

$$\phi_c(r_i) = \sum_{i'=1}^{2N} G_i(r_i - r_{i'})\,\rho_c(r_{i'})$$

$$\boxed{G_i(r,r') = \int G_s(r,r')\,dr'}$$

integrated Green function

$$\boxed{G_s(x,y,z) = 1/\sqrt{(x^2+y^2+z^2)}}$$

standard Green function

Integrated Green's function is needed for modeling large aspect ratio beams!

(O(N log N))

Comparison between the IG and SG for a beam with aspect ratio of 30

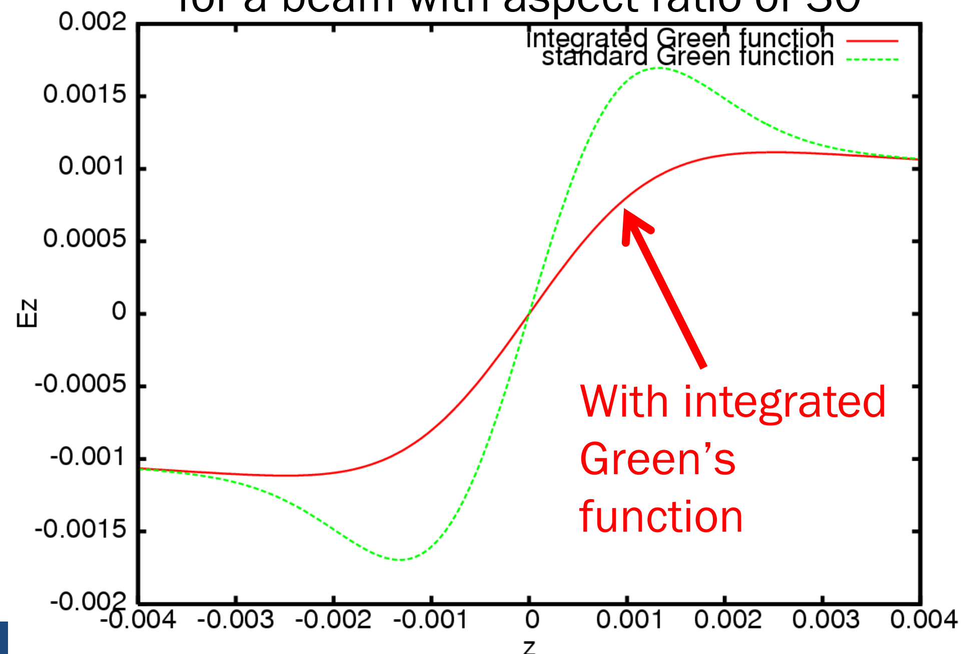

J. Qiang, S. Lidia, R. D. Ryne, and C. Limborg-Deprey, Phys. Rev. ST Accel. Beams, vol 9, 044204 (2006).

3D Poisson Solver with Transverse Rectangular Pipe (I)

$$\frac{\partial^2\phi}{\partial x^2}+\frac{\partial^2\phi}{\partial y^2}+\frac{\partial^2\phi}{\partial z^2}=-\frac{\rho}{\epsilon_0}$$

with boundary conditions

$$\begin{aligned}\phi(x=0,y,z)&=0,\\ \phi(x=a,y,z)&=0,\\ \phi(x,y=0,z)&=0,\\ \phi(x,y=b,z)&=0,\\ \phi(x,y,z=\pm\infty)&=0,\end{aligned}$$

$$\rho(x,y,z)=\sum_{l=1}^{N_l}\sum_{m=1}^{N_m}\rho^{lm}(z)\sin(\alpha_l x)\sin(\beta_m y),$$

$$\phi(x,y,z)=\sum_{l=1}^{N_l}\sum_{m=1}^{N_m}\phi^{lm}(z)\sin(\alpha_l x)\sin(\beta_m y),$$

where

$$\rho^{lm}(z)=\frac{4}{ab}\int_0^a\int_0^b\rho(x,y,z)\sin(\alpha_l x)\sin(\beta_m y),$$

$$\phi^{lm}(z)=\frac{4}{ab}\int_0^a\int_0^b\phi(x,y,z)\sin(\alpha_l x)\sin(\beta_m y),$$

$$\frac{\partial^2\phi^{lm}(z)}{\partial z^2}-\gamma_{lm}^2\phi^{lm}(z)=-\frac{\rho^{lm}(z)}{\epsilon_0},$$

$$\frac{\phi_{n+1}^{lm}-2\phi_n^{lm}+\phi_{n-1}^{lm}}{h_z^2}-\gamma_{lm}^2\phi_n^{lm}=-\frac{\rho_n^{lm}}{\epsilon_0},$$

$$\begin{aligned}\phi_{-1}^{lm}&=\exp(-\gamma_{lm}h_z)\phi_0^{lm}, && n=0,\\ \phi_{N+1}^{lm}&=\exp(-\gamma_{lm}h_z)\phi_N^{lm}, && n=N.\end{aligned}$$

Numerical Solutions vs. Analytical Solutions

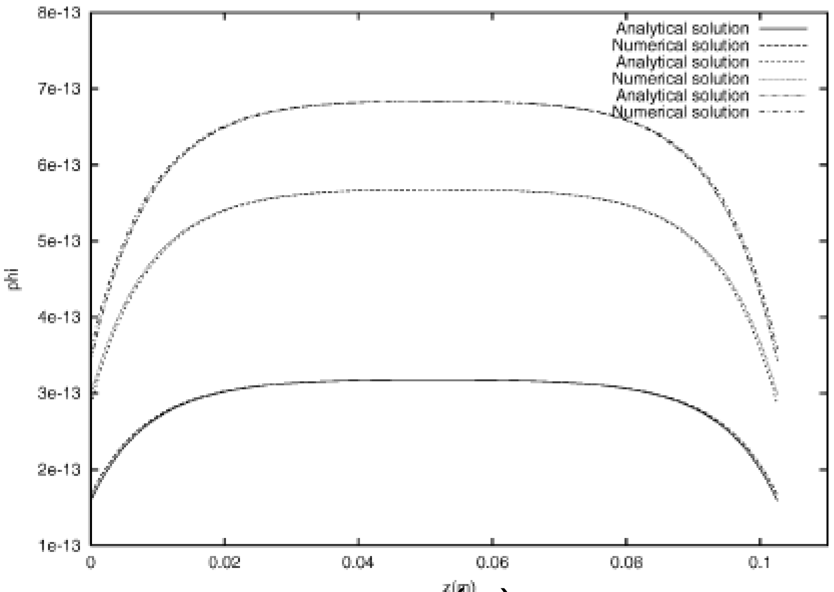

z (m)

J. Qiang, and R. Ryne, Comput. Phys. Comm. 138, p. 18 (2001).

3D Poisson Solver with Transverse Rectangular Pipe (II)

(Spectral-Green Function Method and Spectral Method)

$$\frac{\partial^2 \phi^{lm}(z)}{\partial z^2} - \gamma_{lm}^2 \phi^{lm}(z) = -\frac{\rho^{lm}(z)}{\epsilon_0},$$

Green function method

$$\phi^{lm}(z) = \frac{-1}{2\gamma_{lm}\varepsilon_0} \int \exp(-\gamma_{lm} |z - z'|) \rho^{lm}(z') dz'$$

$$\phi^{lm}(z) = \frac{-1}{2\gamma_{lm}\varepsilon_0} \sum_j \rho^{lm}(z_j') G(z - z_j')$$

$$G(z - z') = \int_{z'-h/2}^{z'+h/2} \exp(-\gamma_{lm} |z - t|) dt$$

spectral method

$$\phi^{lm}(z) = \sum_n \phi_n^{lm} H_n(z); \; \rho^{lm}(z) = \sum_n \rho_n^{lm} H_n(z)$$

$$\int_{-\infty}^{\infty} H_n(z) H_m(z) dz = 2^n n! \sqrt{\pi} \delta_{mn}$$

$$\frac{1}{4}\phi_{n-2}^{lm} - \left(\frac{1}{2}(2n+1) + \gamma_{lm}^2\right)\phi_n^{lm} + (n+2)(n+1)\phi_{n+2}^{lm} = A^2 \rho_n^{lm}$$

J. Qiang, in Proc. of HB2014.

Space-Charge Driven Energy Modulation vs. Distance in a Drift Space

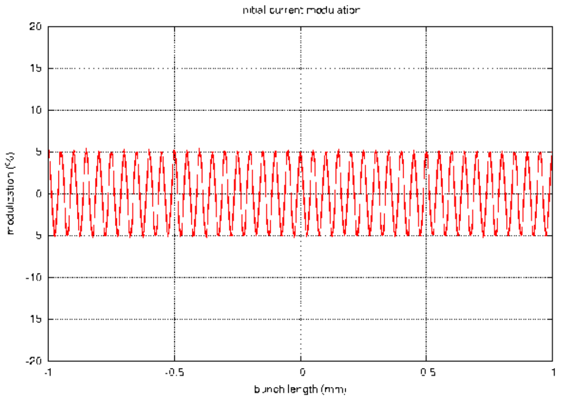

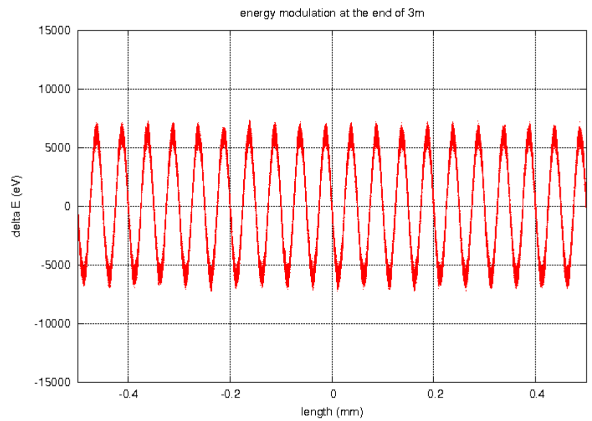

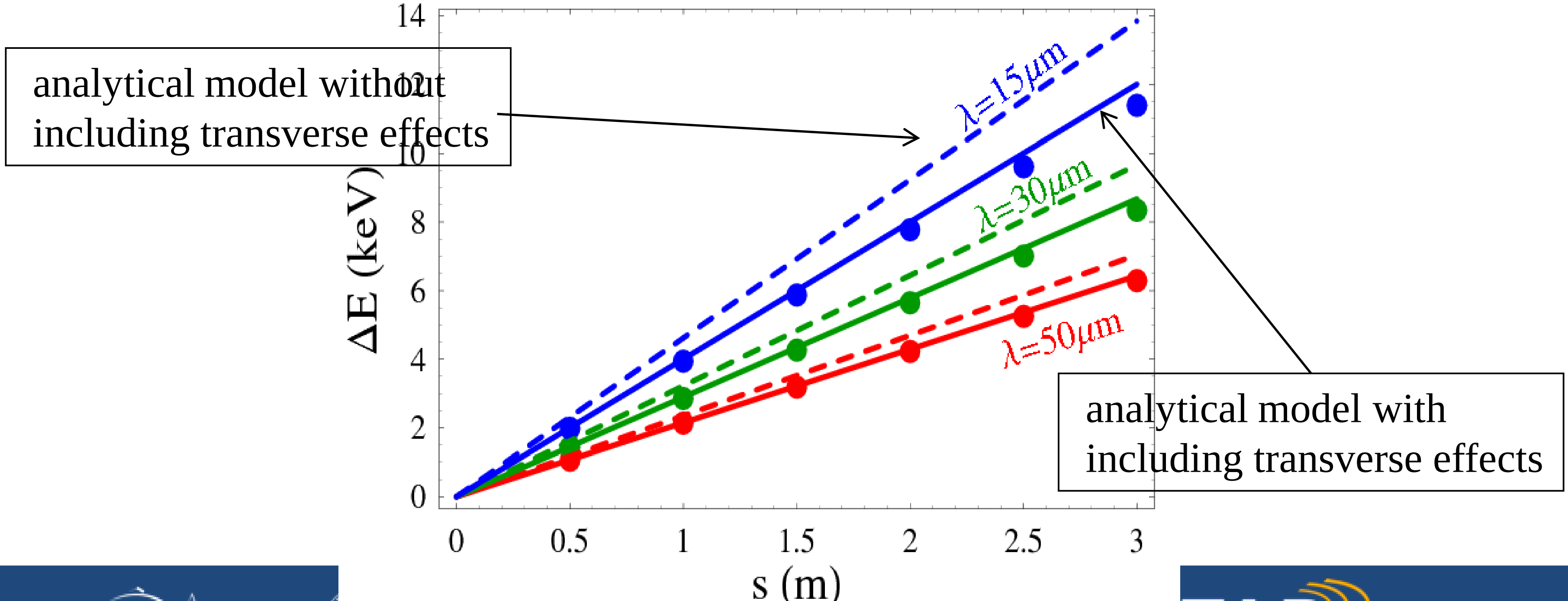

Efficient Method to Calculate Longitudinal and Transverse Wakefields

$$F_x(s) = q\int_s^{+\infty} W_T(s-s')x(s')\lambda(s')ds'$$

$$F_z(s) = \int_s^{+\infty} W_L(s-s')\lambda(s')ds'$$

$$F(s) = \int_{-\infty}^{+\infty} G(s-s')\rho(s')ds'$$

$$G(s) = \begin{cases} W(s) & for\ s \geq 0 \\ 0 & for\ s < 0 \end{cases}$$

$$F_c(s_i) = h\sum_{i'=1}^{2N} G_c(s_i - s_{i'})\rho_c(s$$

$$F(s_i) = F_c(s_i) \quad for\ i = 1,\ldots N$$

Operations comparison using
the direct summation and the FFT based method

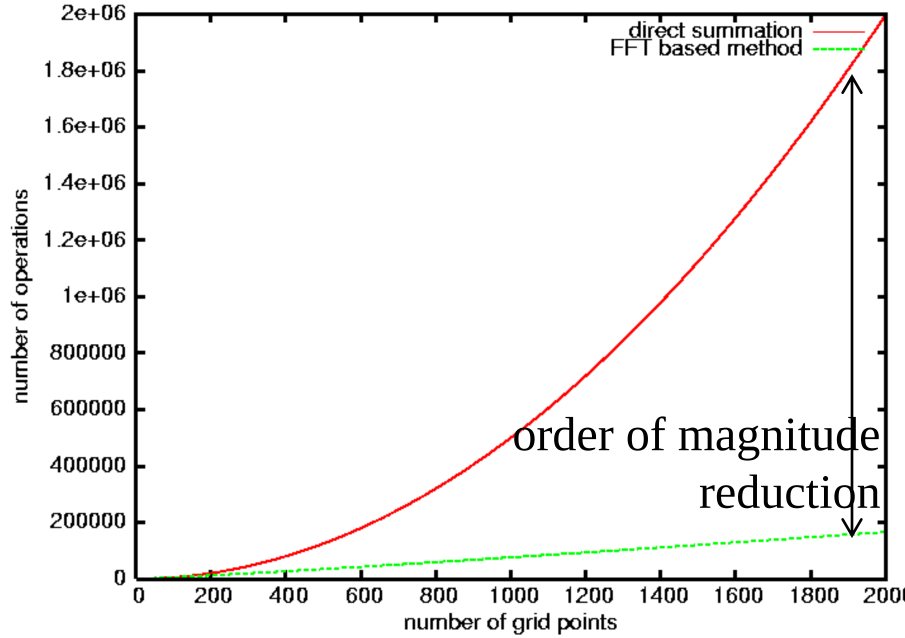

~~direct summation ($O(N^2)$)~~

FFT based ($O(N\log(N))$)

J. Qiang et al., Phys. Rev. ST Accel. Beams, 12, 100702 (2009).

Efficient Integrated Green Function (IGF) Method to Calculate Longitudinal (CSR) Wakefield

typical CSR calculation:

a)no short-range interaction

b)with numerical filtering

$$E(s) = -\int ds' \frac{d\lambda(s')}{ds'} \nu(s-s')$$

new IGF based method :

$$E(s) = \int dz' \lambda(s') w(s-s'),$$

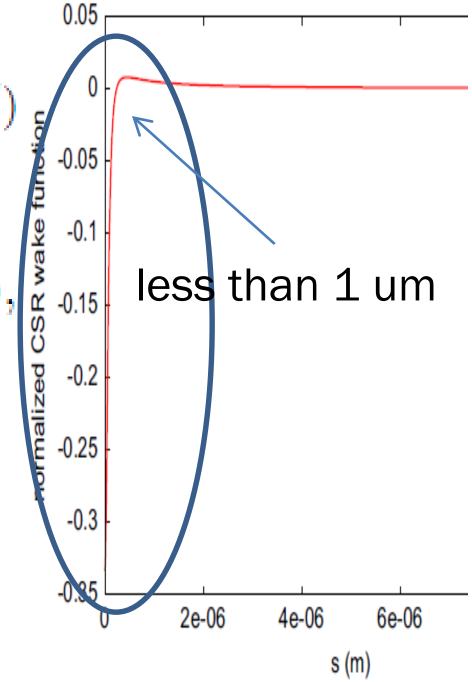

$$W(u(s)) = \frac{1}{4\pi\epsilon}\frac{\gamma^4}{R^2}\left\{\frac{u^2/4-1}{2(1+u^2/4)^3} + \frac{1/6 - u^2/18 - u^4/64}{(1+u^2/4)^3(1+u^2/12)^2}\right\}$$

New method with integrated Green's function method :

$$\boxed{v_i(r,r') = \oint w_s(r,r')dr'}$$

$$E_c(r_i) = \sum_{i'=1}^{2N} v_i(z_i - z_{i'})\rho_c(z_{i'})$$

$$\int_{z_j-h_{int}/2}^{z_j+h_{int}/2} W(z-z')dz' = [\nu(A(z-z_j+h_{int}/2)) - \nu(A(z-z_j-h_{int/2}))]/A$$

$$\nu(u) = -\frac{e\gamma^4}{4\pi\epsilon R^2}\frac{3}{4}\left\{-\frac{2}{u} + \frac{1}{u\sqrt{u^2+1}}(\Omega^{1/3}+\Omega^{-1/3}) + \frac{2}{\sqrt{u^2+1}}(\Omega^{2/3}-\Omega^{-2/3})\right\}$$

J. Qiang, et. al, NIMA 682, 49 (2012).

IGF Significantly Reduces the Numerical Grid Points:

A Comparison in 1-D models with Transient Effects

1nC, 50 μm Gaussian bunch at 150 MeV; bend with radius R = 1.5 m*

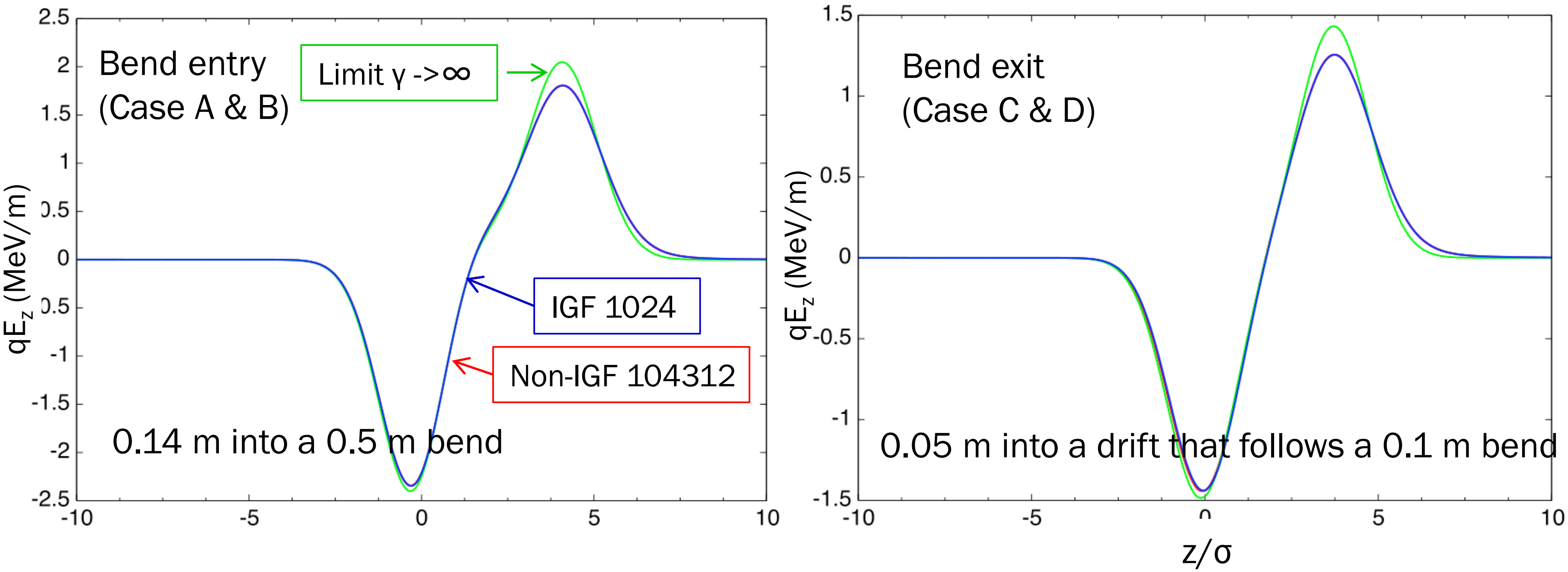

IGF method obtains the same accuracy as direct integration with a factor of 100 fewer sample points

IGF 1024 points
Non-IGF 104312 points
Limit $\gamma \rightarrow \infty$

*G. Stupakov and P. Emma, Proc. EPAC 2002, Paris, France, 1479 (2002).

C. Mitchell, et. al, NIMA 715, 119 (2013).

Modeling the Photo-Electron Emission from Three Step Model

(Includes both Material and External Schottky Work Function Effects)

- photo-electron beam quality born out of the photo-cathode sets the limit of the final beam brightness for next generation light sources

Three-Step Photo-Emission Model

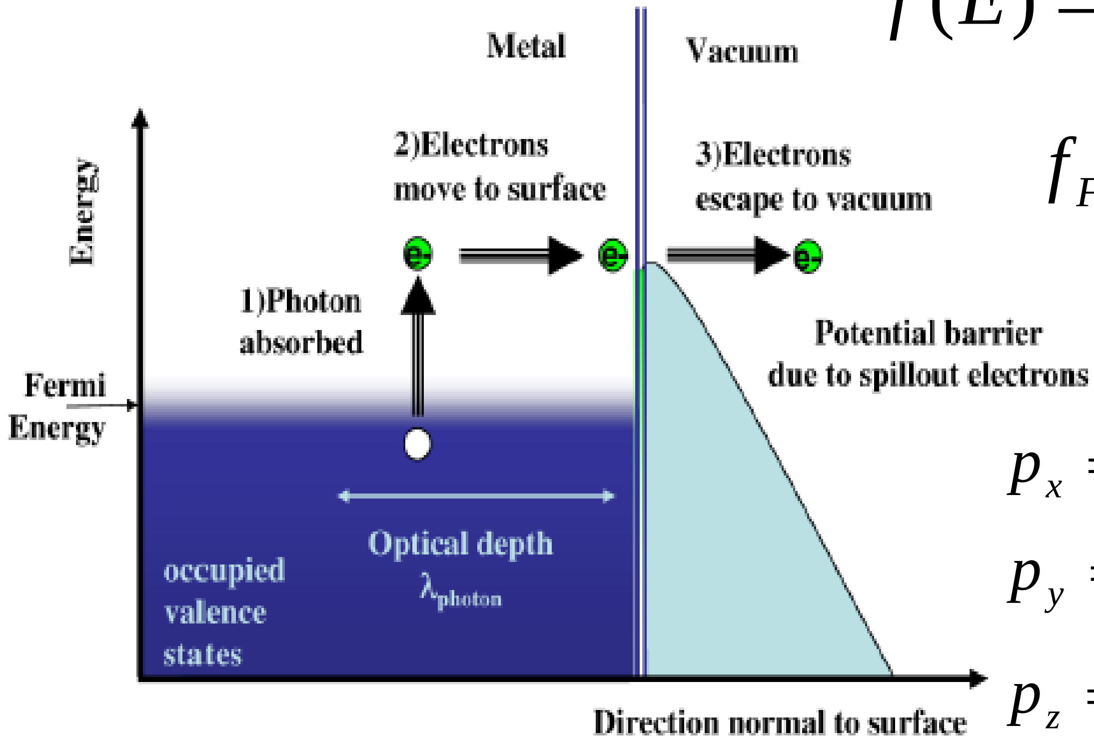

$$f(E) = (1 - f_{FD}(E))\, f_{FD}(E - h\nu)$$

$$f_{FD}(E) = \frac{1}{1 + e^{(E - E_F)/k_B T}}$$

$$f(\theta, \phi) = \sin(\theta)$$

$$p_x = \sqrt{2mE}\,\sin(\theta)\cos(\phi)$$

$$p_y = \sqrt{2mE}\,\sin(\theta)\sin(\phi)$$

$$p_z = \sqrt{2m(E - E_F - \phi_{eff}) - p_x^2 - p_y^2}$$

D. Dowell et al., PRSTAB 2009.

A 2nd Order Numerical Model to Simulate Photo-Emission Significantly Reduces the Number of Emission Steps

photocathode

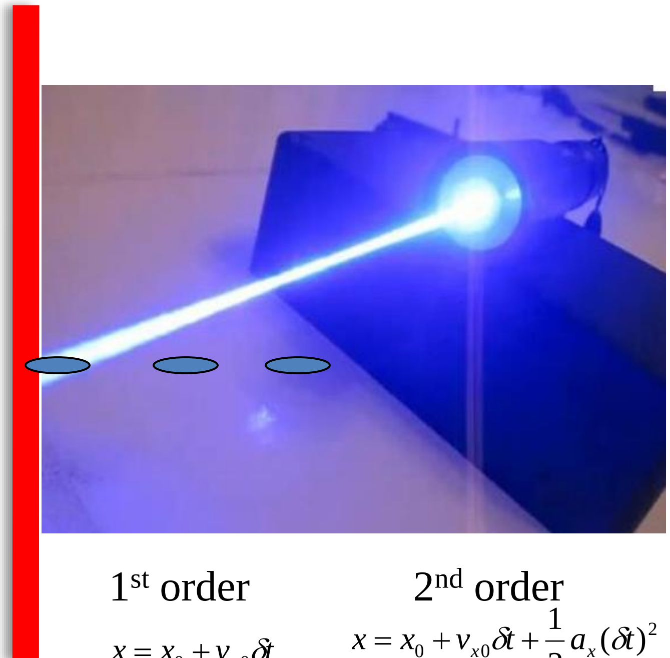

1st order

$$x = x_0 + v_{x0}\delta t$$
$$v_x = v_{x0}$$
$$z = v_{z0}\delta t$$
$$v_z = v_{z0}$$

2nd order

$$x = x_0 + v_{x0}\delta t + \frac{1}{2}a_x(\delta t)^2$$
$$v_x = v_{x0} + a_x\delta t$$
$$z = v_{z0}\delta t + \frac{1}{2}a_z(\delta t)^2$$
$$v_z = v_{z0} + a_z\delta t$$

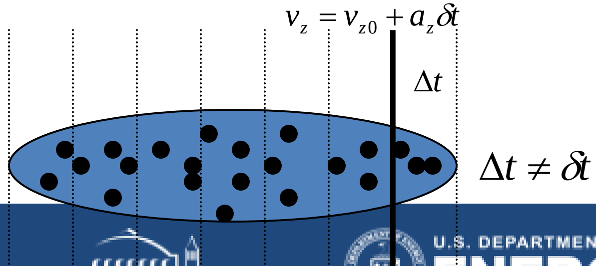

Current Profile with Different Number of Emission Steps (2nd order vs. 1st order emission model)

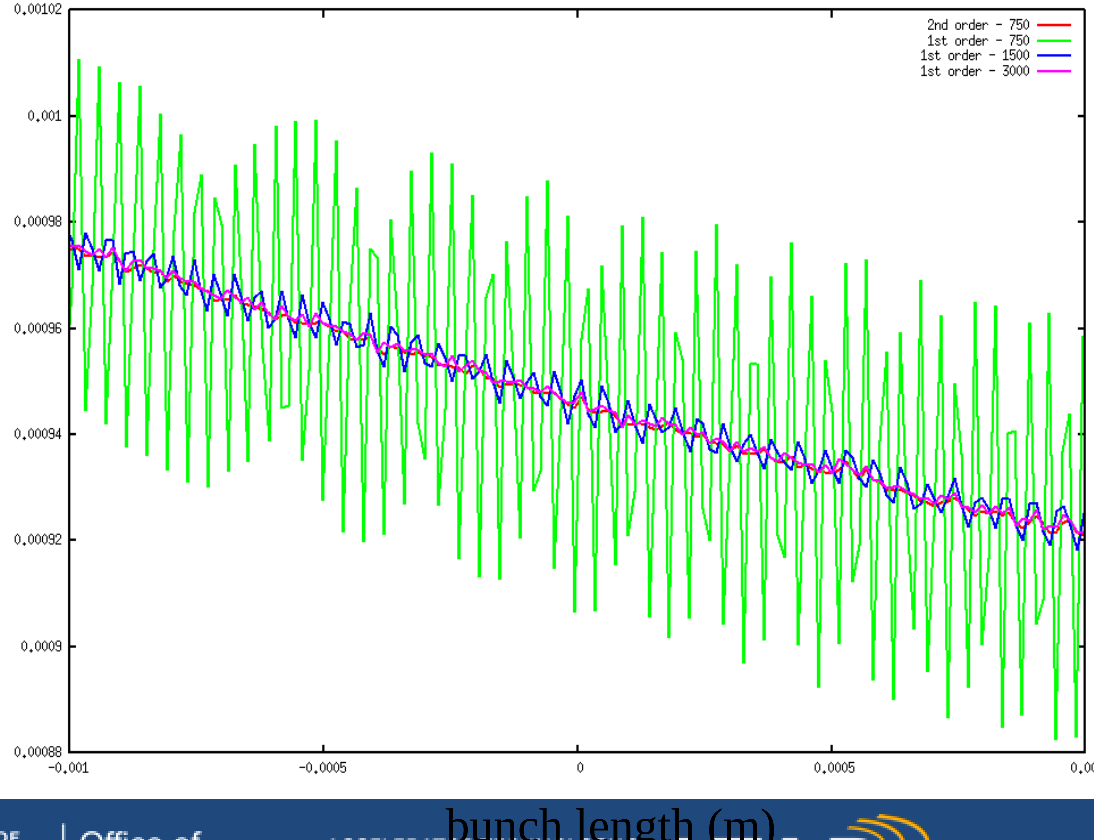

Some Application Examples

Modeling of the ALS Streak Camera Using IMPACT – with Space Charge Effects

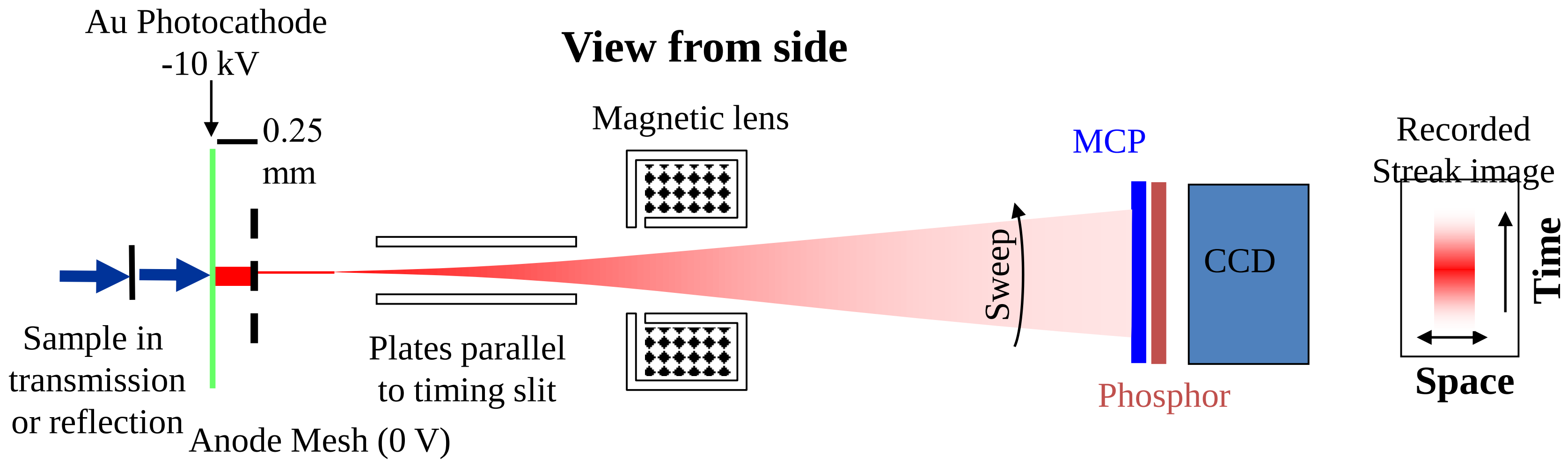

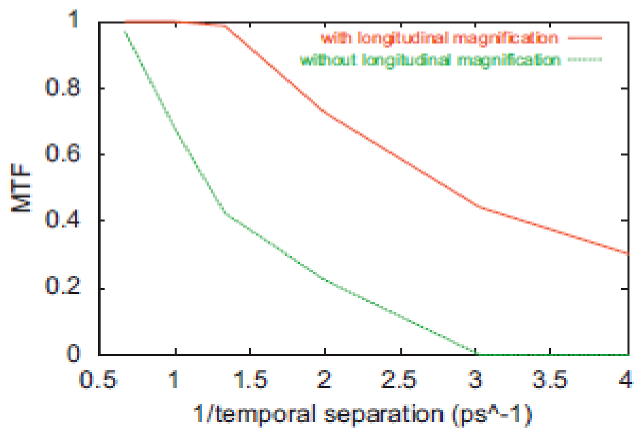

X-ray streak camera temporal reslution improvement using a longitudinal time-dependent field

Space-Charge Effects in Streak Camera

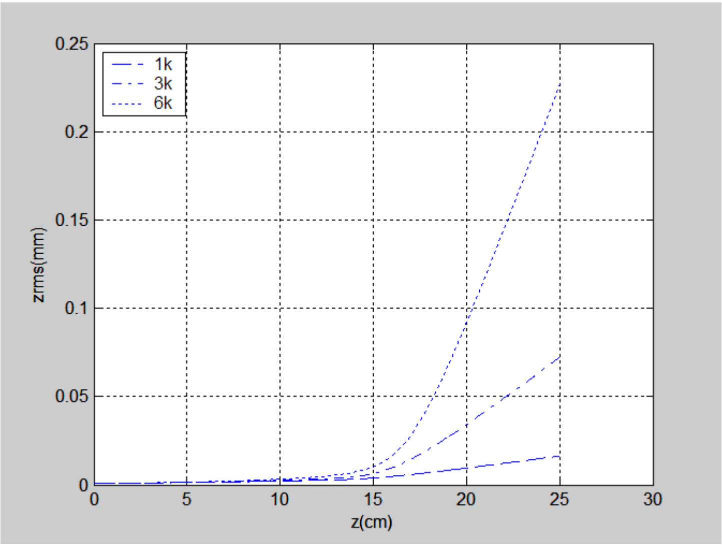

J. Qiang et al., Nuclear Instruments & Methods in Physics Research A 598, 465 (2009).
J. Feng, et. al, Proceedings of SPIE, Vol.5920, 592009 (2005).

A Movie Showing the Dynamics of Field Emission Dark Current and Transport in the Injector

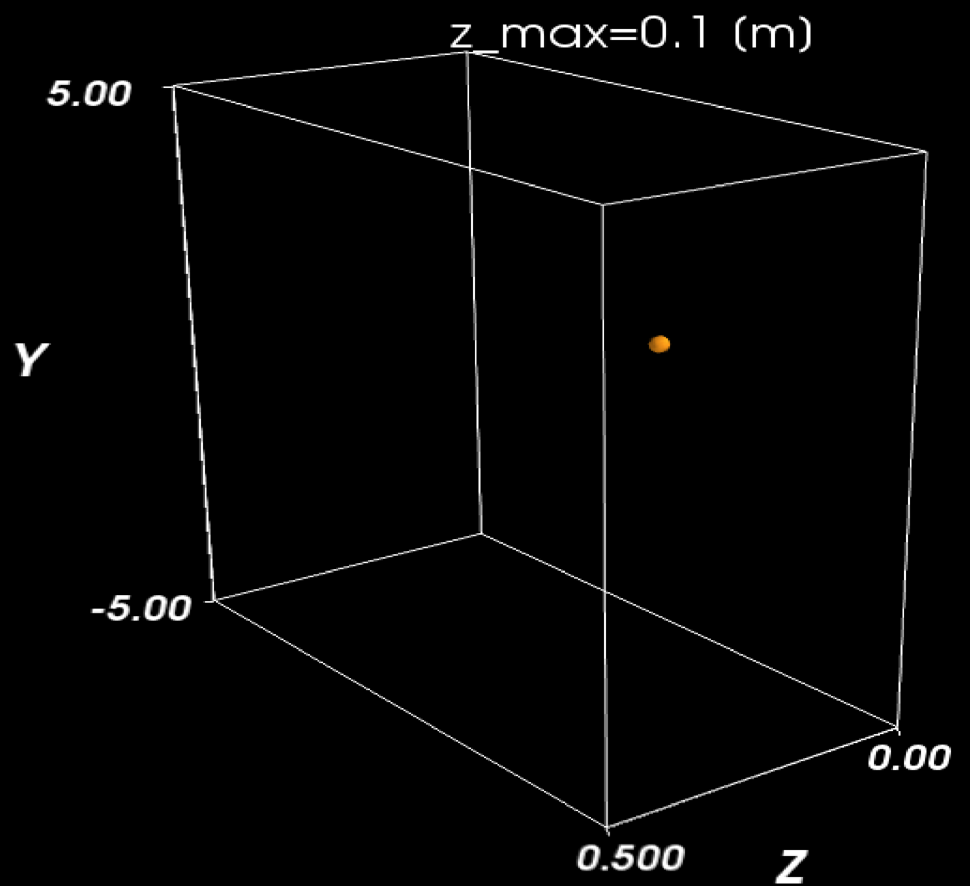

A Movie Showing Dark Current Halo Electrons Transport/Get Lost Using Field Data from Unstructured Grid

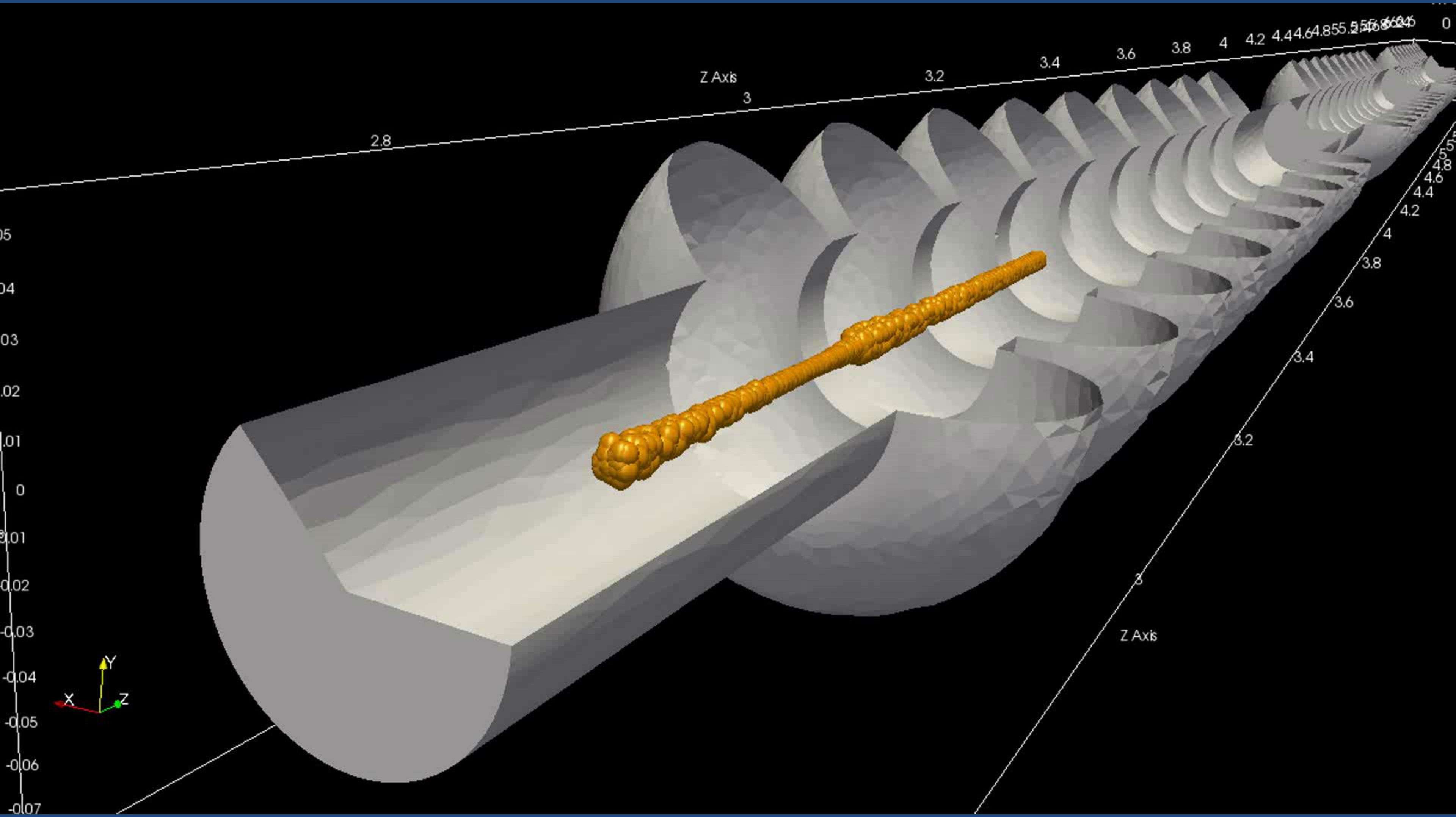

Integration of Parallel Multi-Objective Optimization with Parallel Beam Dynamics Simulation of a Photo-Injector

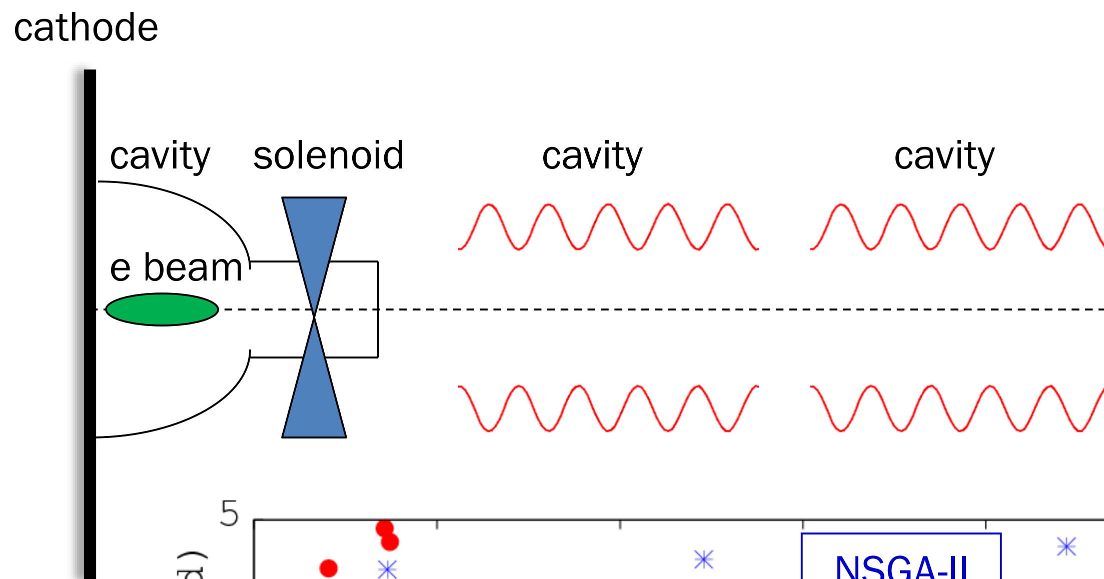

Control Parameters (10):

Initial laser transverse size and pulse length (2)
Gun cavity phase (1)
Solenoid strength and position (2)
RF module starting position (1)
Cavity 1 phase and amplitude (2)
Cavity 2 phase and amplitude (2)

VPES-PMDE shows much faster convergence than the popular genetic algorithm NSGA-II with 800 function evaluations!

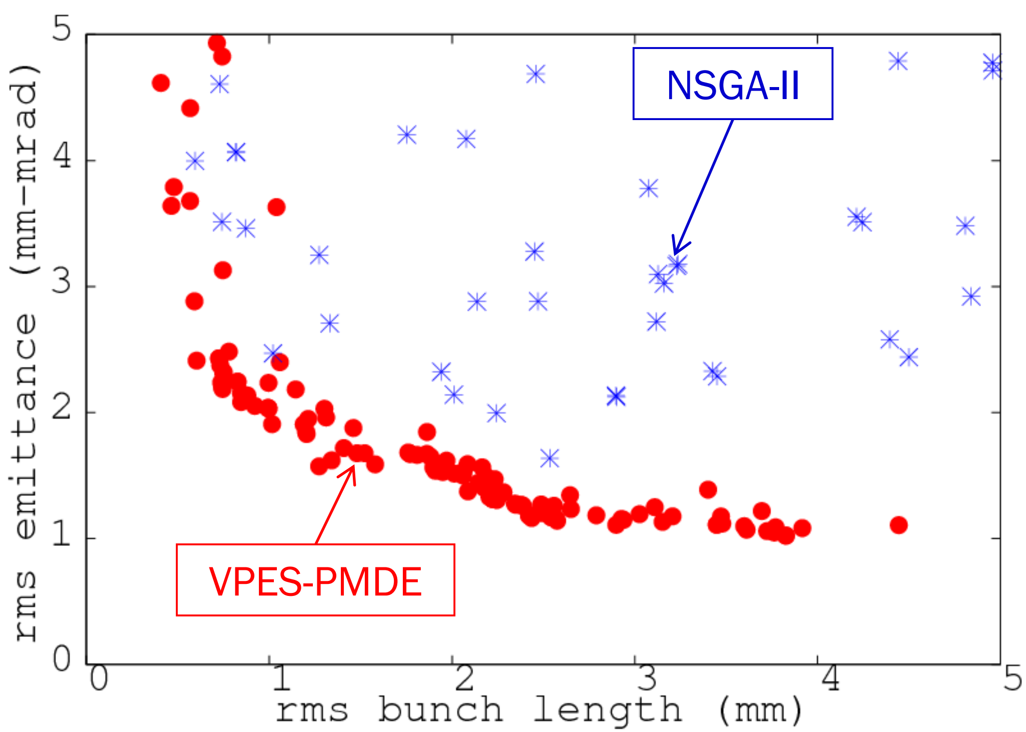

IMPACT Application in Electron Linac for Next Generation Light Sources

Beam manipulation and conditioning

Beam distribution and individual beamline tuning

~2 GeV CW superconducting linac

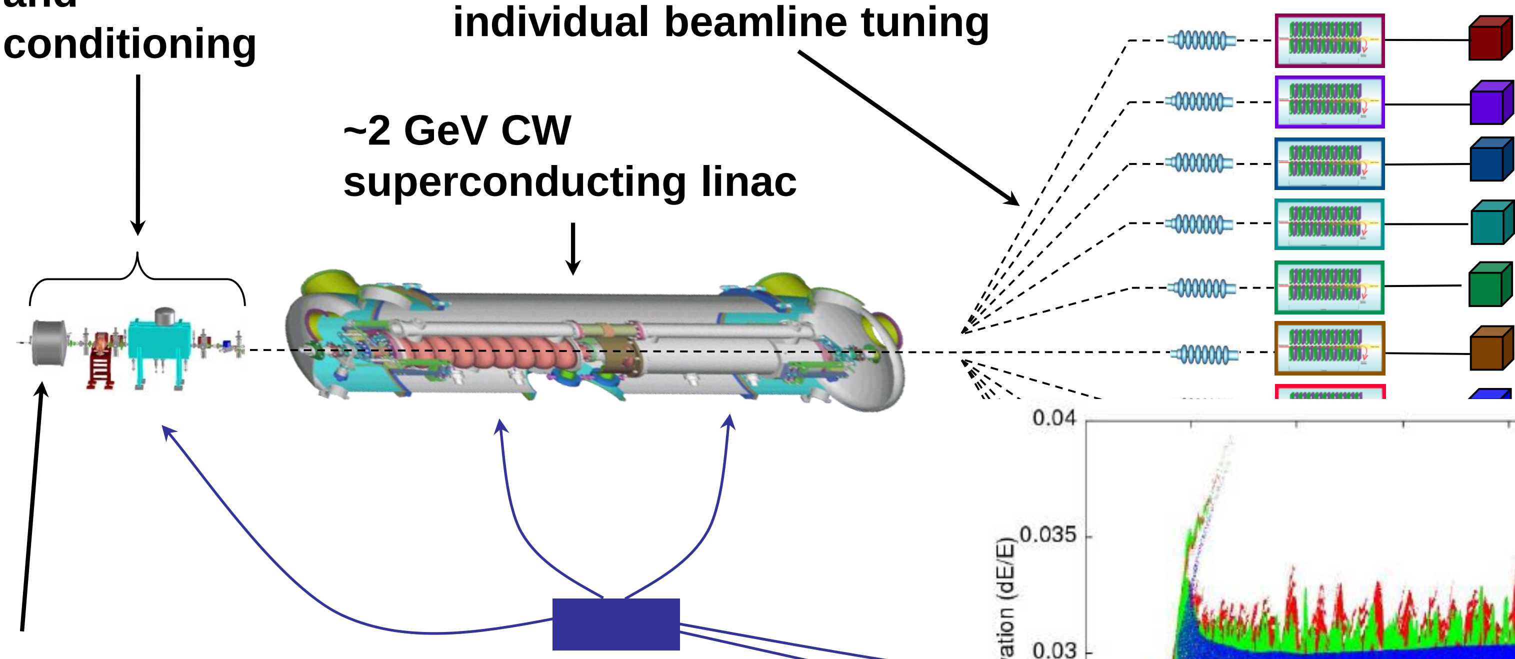

Low-emittance, high rep-rate electron gun

Laser systems, timing & synchronization

FEL Power/undulator length $\sim f\left(I_{peak}, \frac{\varepsilon_n}{\gamma}, \sigma_E\right)$

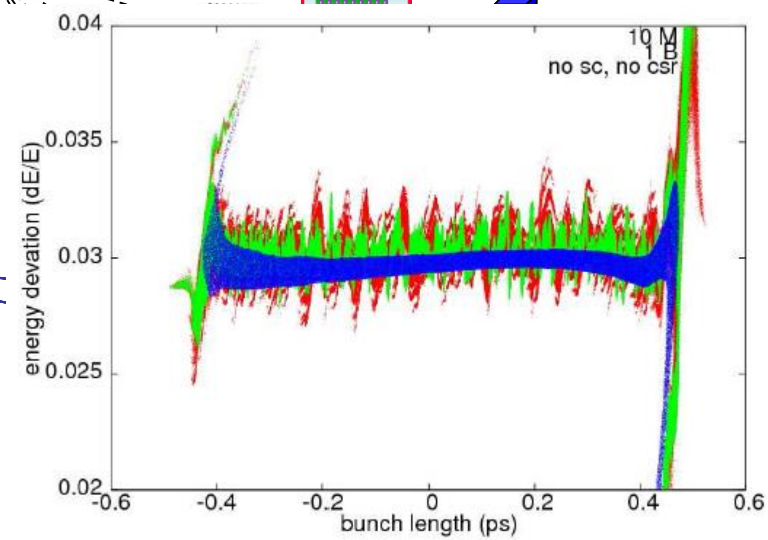

The longitudinal phase space of a beam at the exit of a linac

Longitudinal Space-Charge Effects: Microbunching Instability

• Initial density modulation induces energy modulation through long. impedance Z(k), converted to more density modulation by a chicane ➔ growth of slice energy spread / emittance!

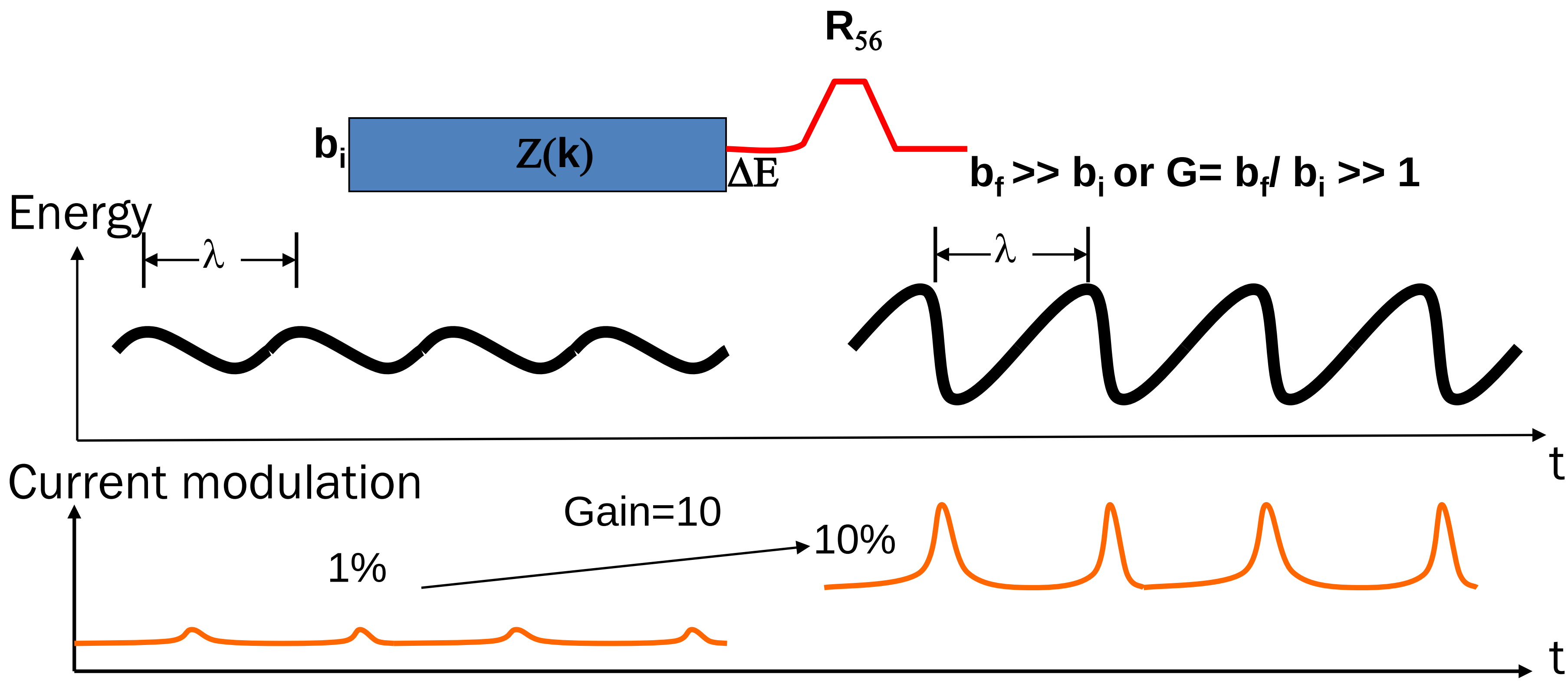

Courtesy of Z. Huang

Modeling the Development of the Microbunching Instability from the Shot Noise

From the exit of BC1 through BC2 in an FEL driver.

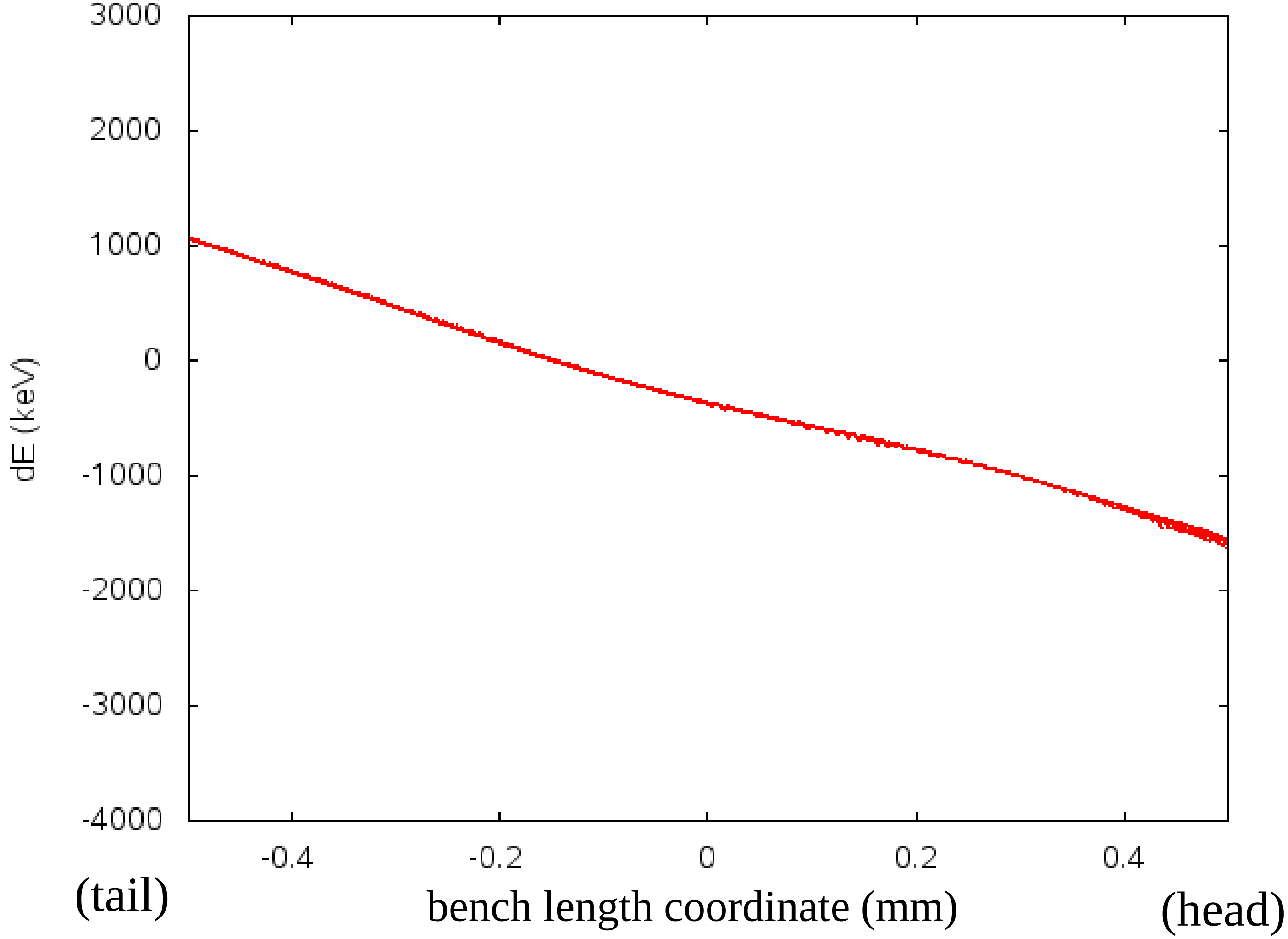

Final Longitudinal Phase Space & RMS Slice Energy Spread

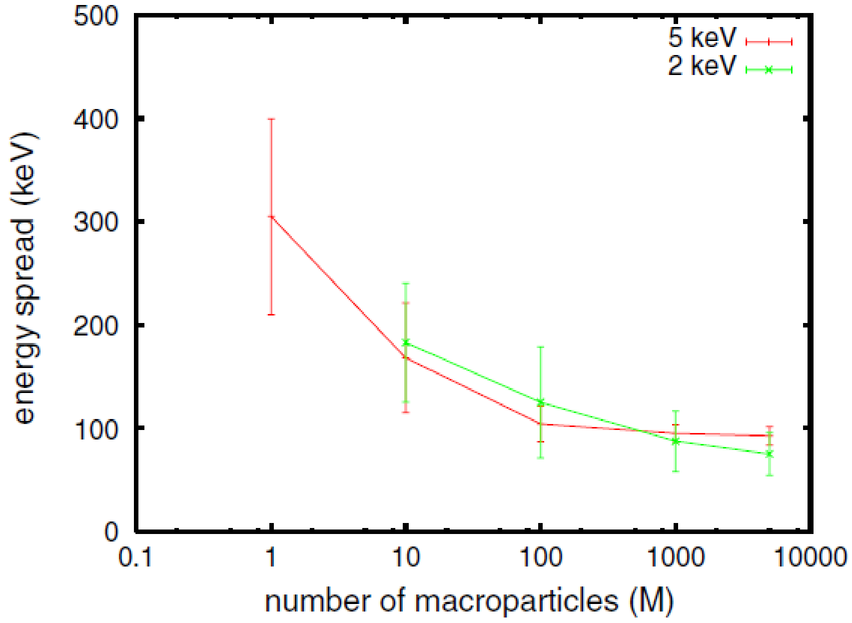

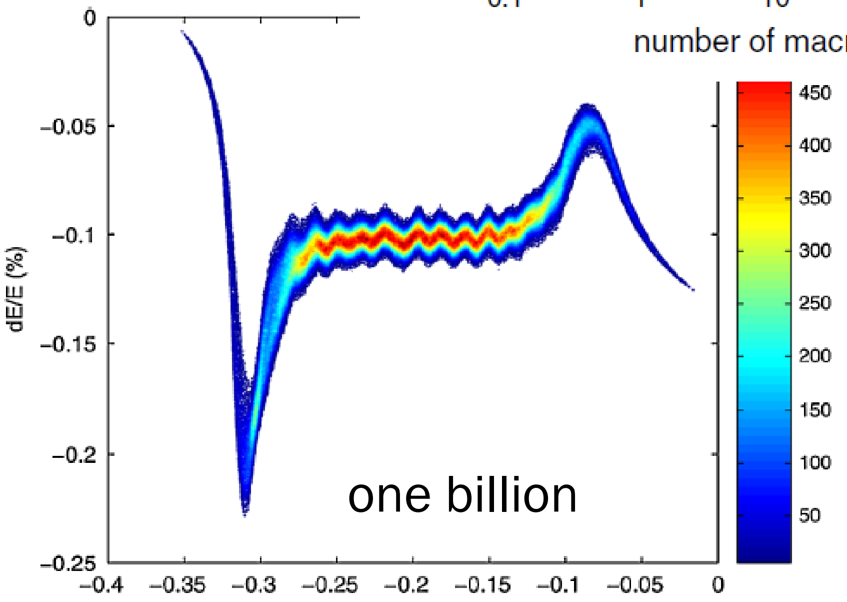

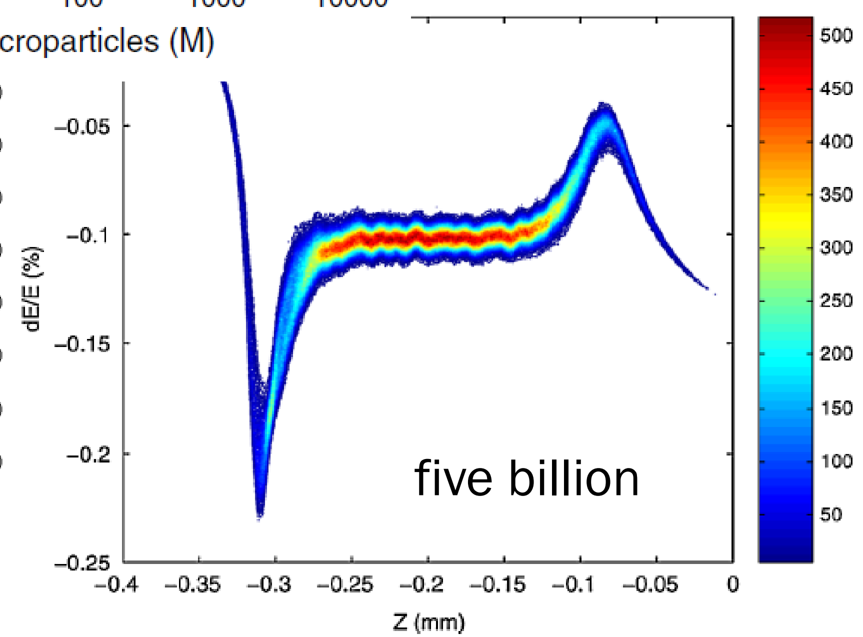

J. Qiang et al., PRST-AB 12, 100702, 2012.

Simulations Reproduce Experimental Observation of uBI: Benchmark IMPACT Simulations vs. LCLS Measurements

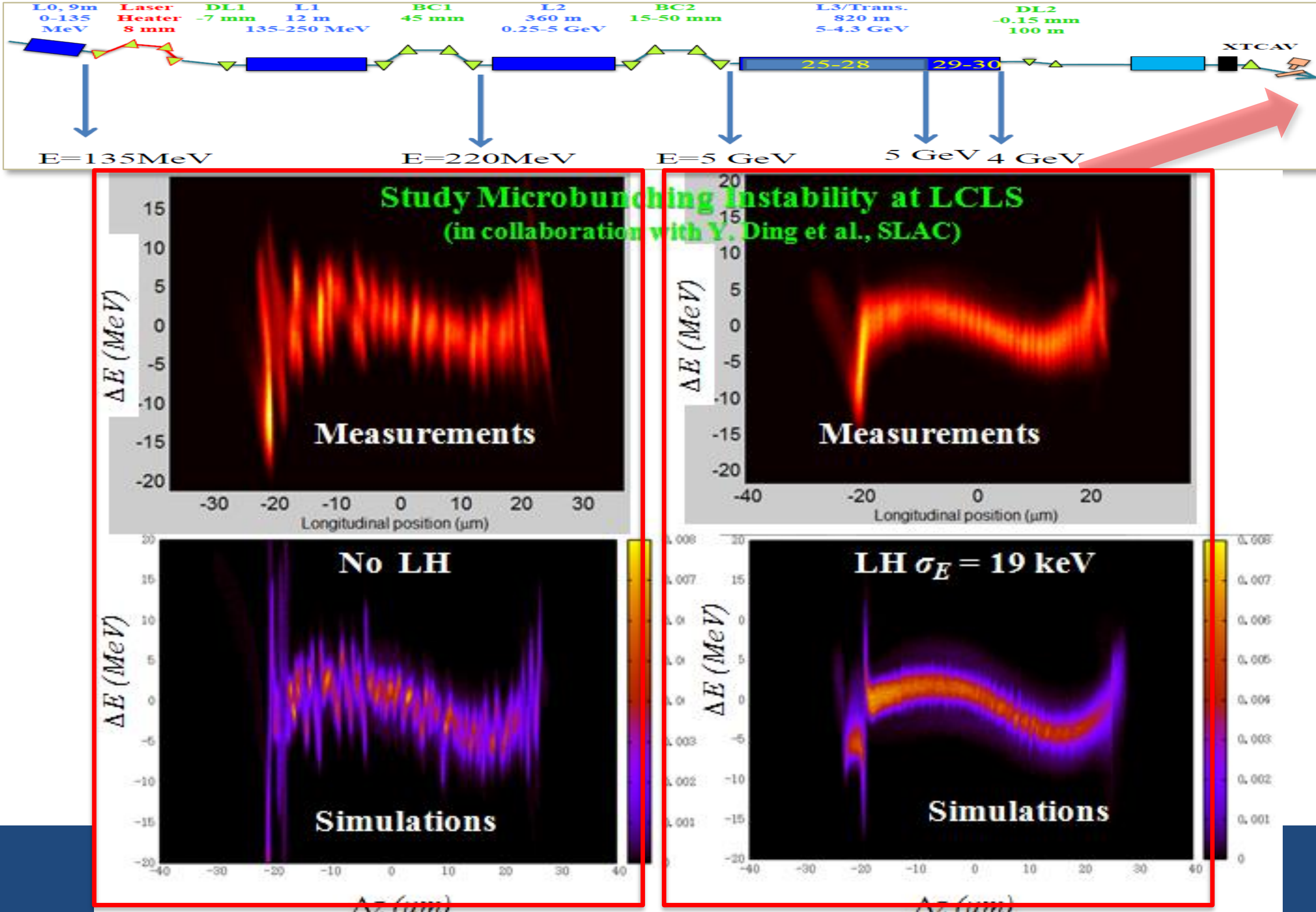

Real Number of Electron Matters : No Need for Shot Noise Model

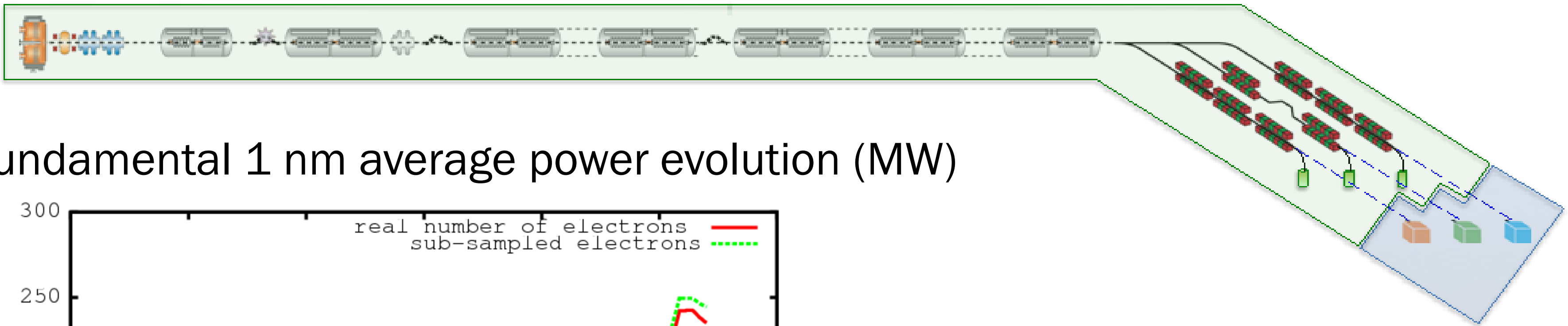

fundamental 1 nm average power evolution (MW)

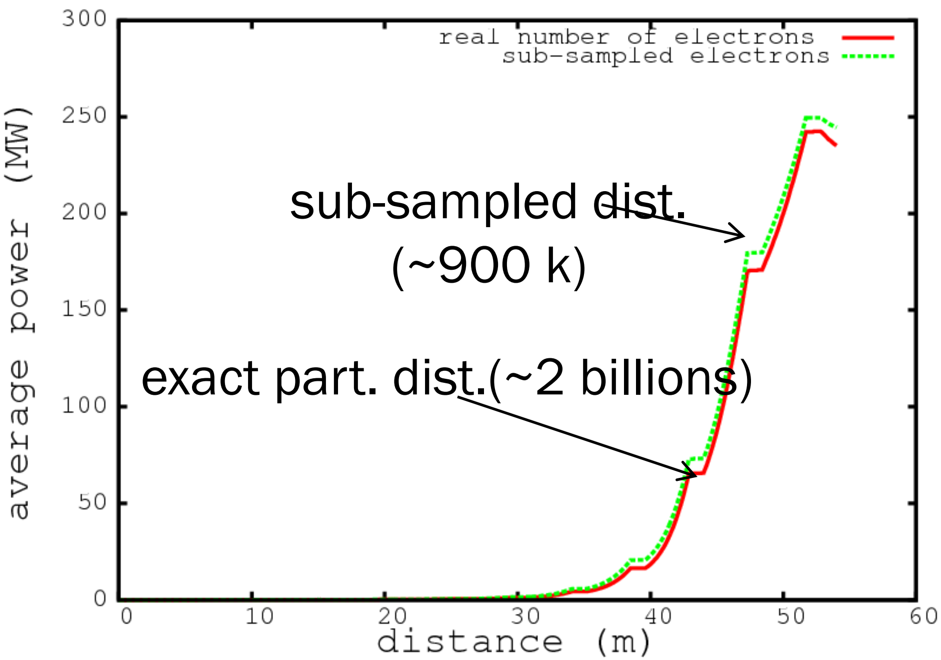

J. Qiang et al., Phys. Rev. ST Accel. Beams, vol. 17, 030701 (2014).

3^{rd} harmonic 0.333 nm average power evolution (MW)

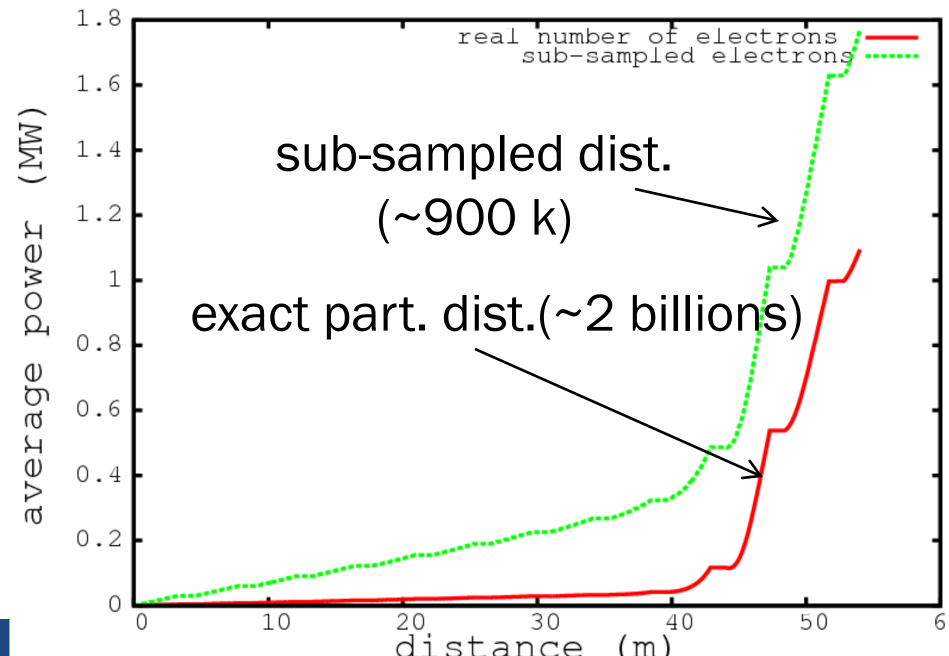

3D Modeling Multi-Charge State Ion Beam Formation and Transport at ECR Ion Source

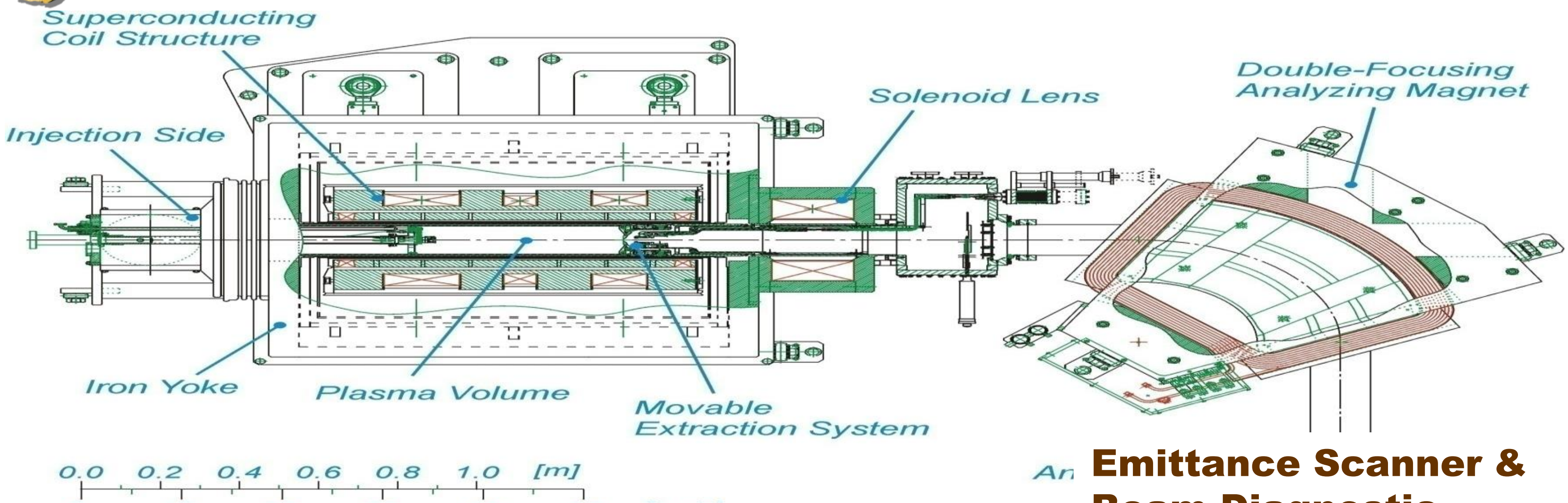

Emittance Scanner & Beam Diagnostic

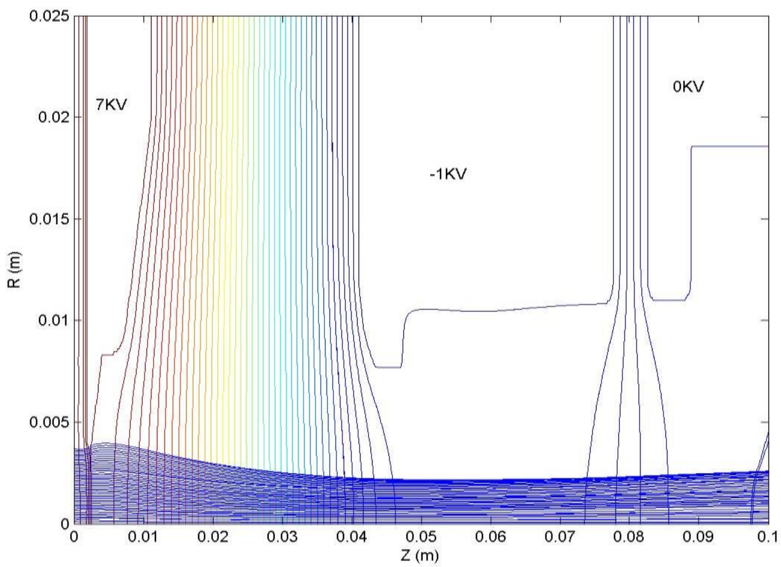

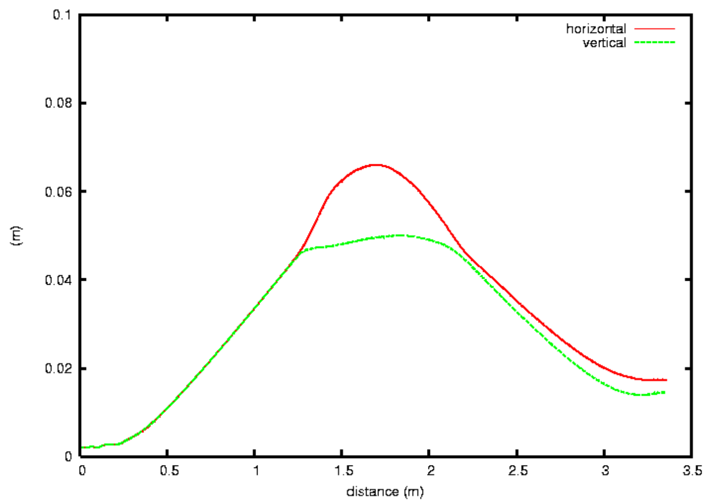

J. Qiang et al, Computer Physics Communications, vol. 175, 416, (2006).

SNS Beam Dynamics Studies: Space-Charge and RF Nonlinearities Required for Accurate Model

IMPACT model and measurement at the MEBT

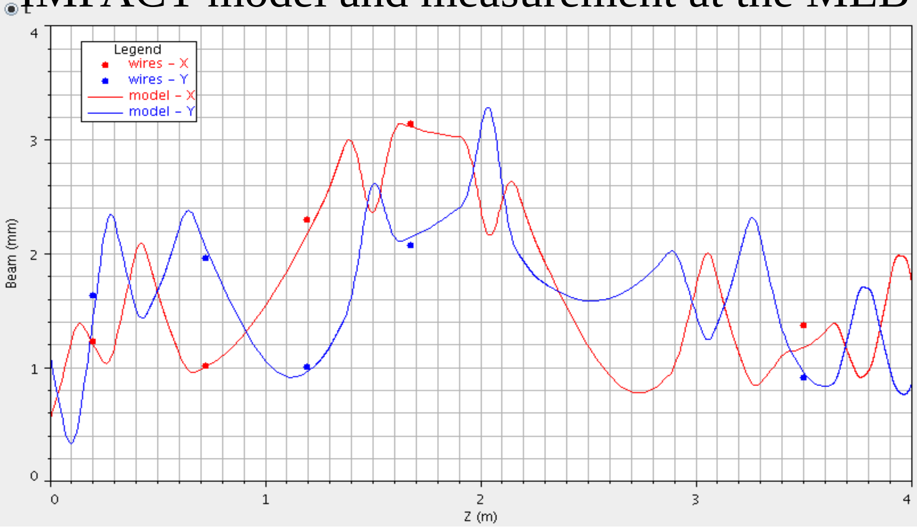

IMPACT model and the LWs measurements in SC linac

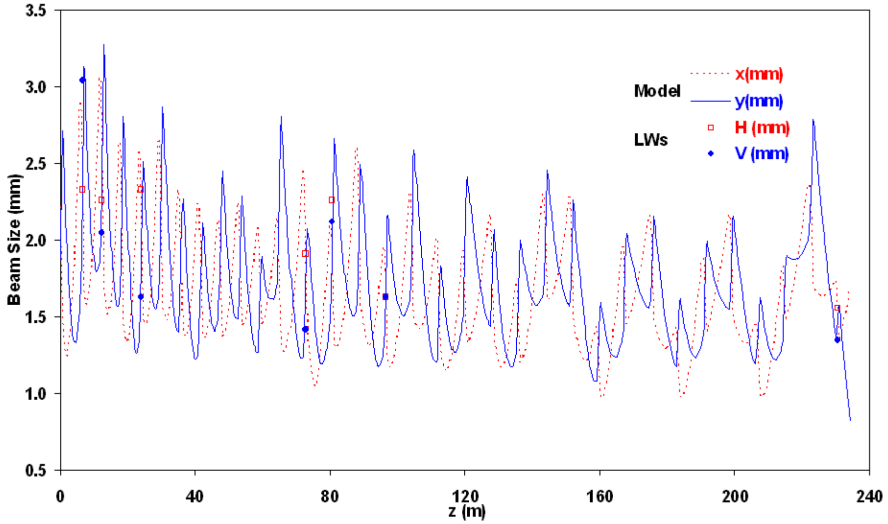

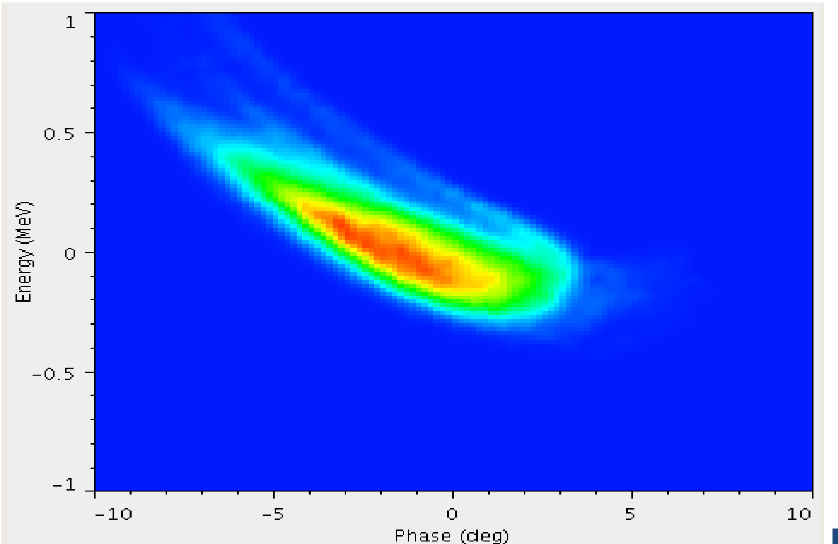

IMPACT model of DTL6 phase shifted by 6°

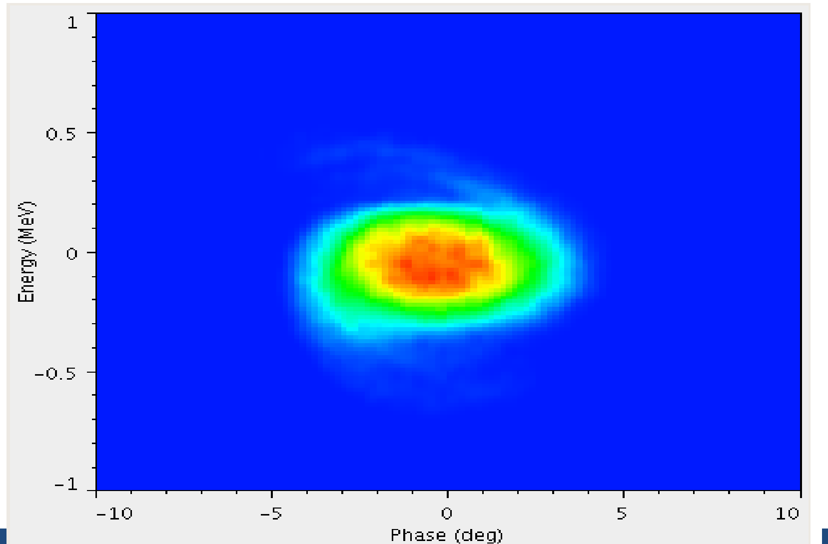

IMPACT predicted profiles at the SCL entrance

Y. Zhang and J. Qiang, PAC09, p. 2653.

Macroparticle Simulation of a Proton Beam Halo Experiment

Evolution of the Normalized Cumulative Beam intensity

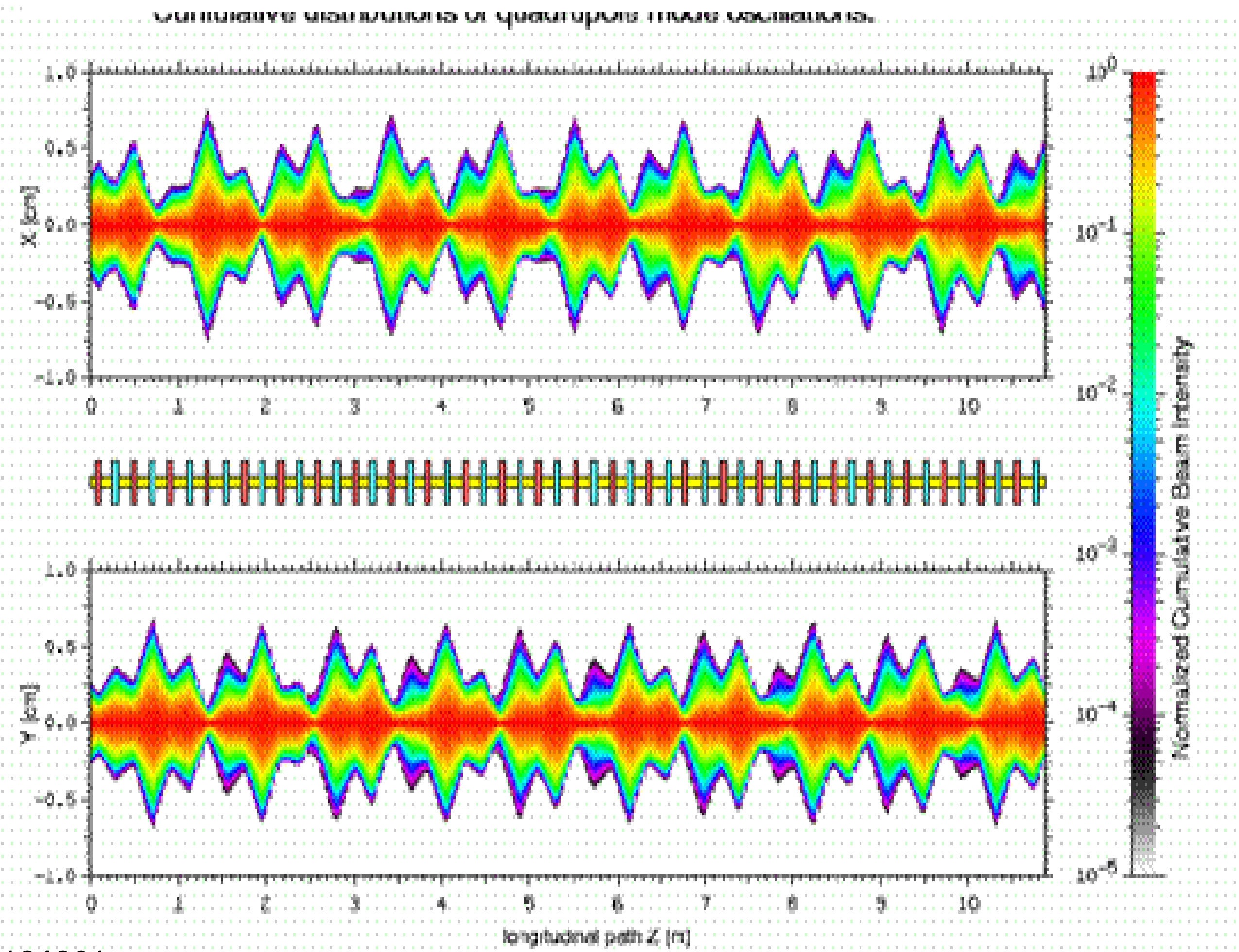

J. Qiang et. al, PRST-AB 5, 124201.

Horizontal Beam Profiles at 9 Wire Scanners Show Good Agreement between Simulations and Measurements

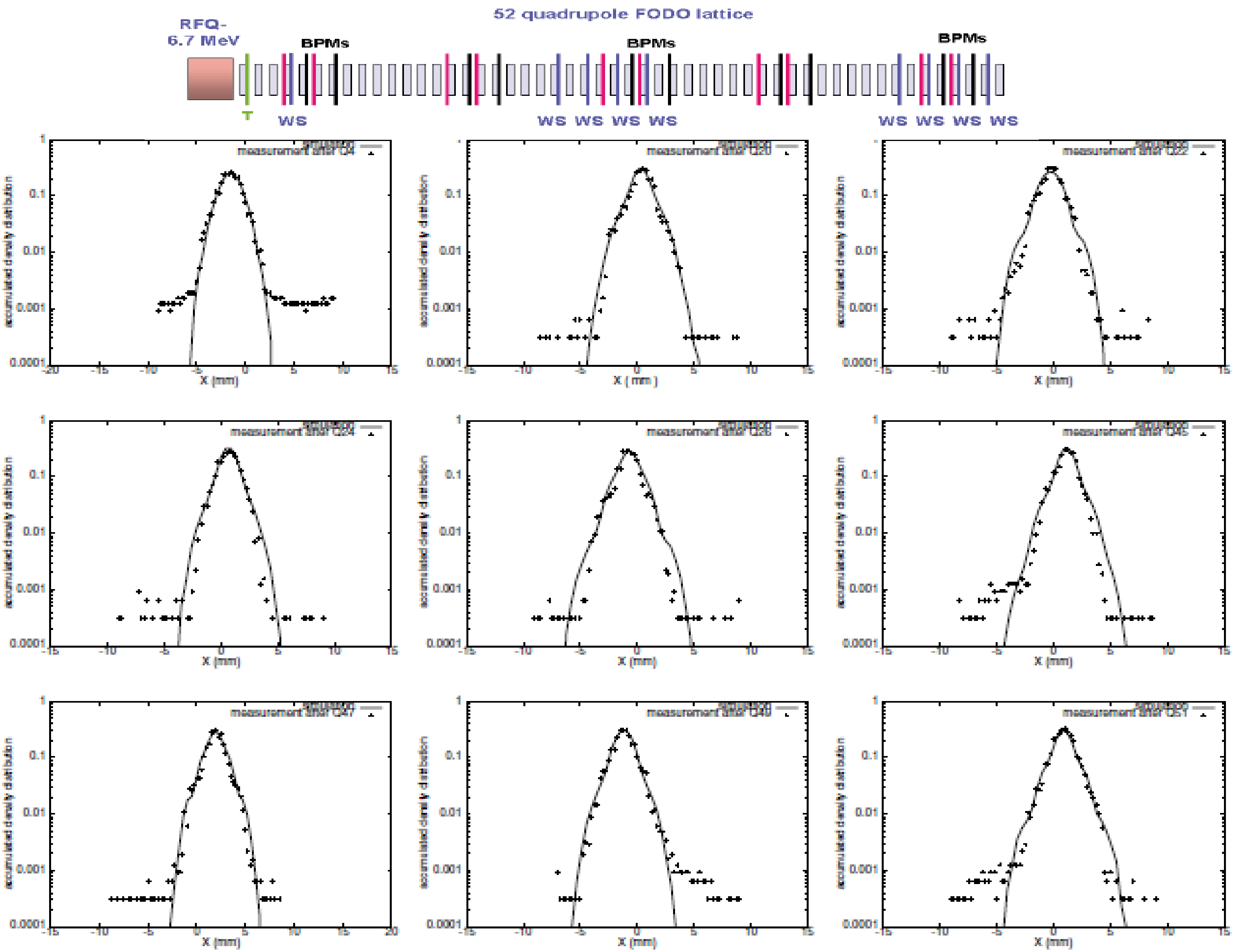

Space-Charge Driven Coupling Resonance at PS

“For this purpose increasing levels of complexity have been planned with simulations, first in 2D approximation and up to 2000 turns:
- step (1) in constant focusing approximation;
- step (2) using a linearized version of the AG lattice;
- step (3) using the fully nonlinear lattice of the PS [7]);
- step (4) the 21/2 D or 3D bunched beam simulation including all lattice effects;
- step (5) extension up to the full 13,000 turns of the measurements provided that necessary CPU times – pre- sumably of the order of months – are not prohibitive.

At a later point, after suitable code optimization, the even more ambitious dynamical crossing may be addressed, preferably after new measurements are carried out over less than the demanding 44.000 turns of the 2003 experiment.” - I. Hofmann et al., Proceedings of 2005 PAC.

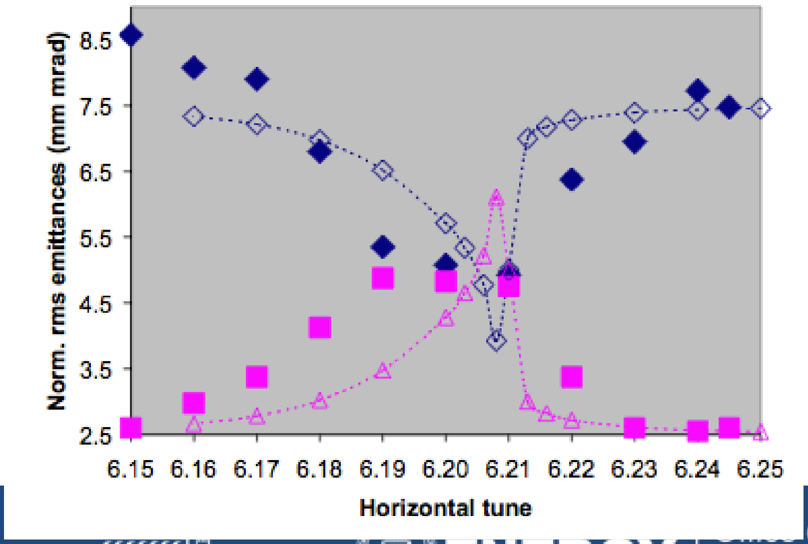

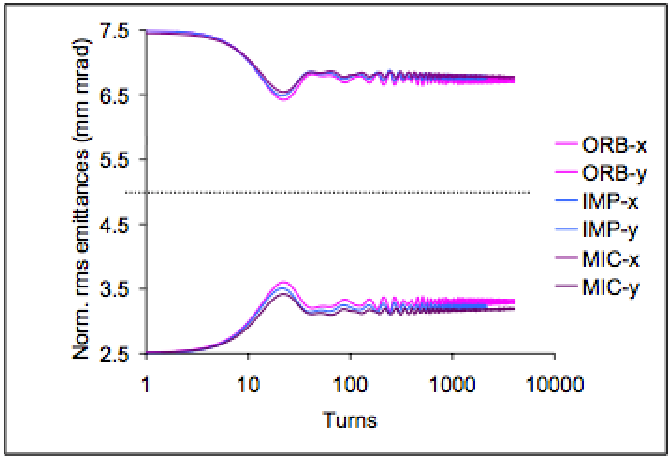

3D IMPACT Simulation Improves Agreement in Static Montague Resonance Crossing at PS

measurements

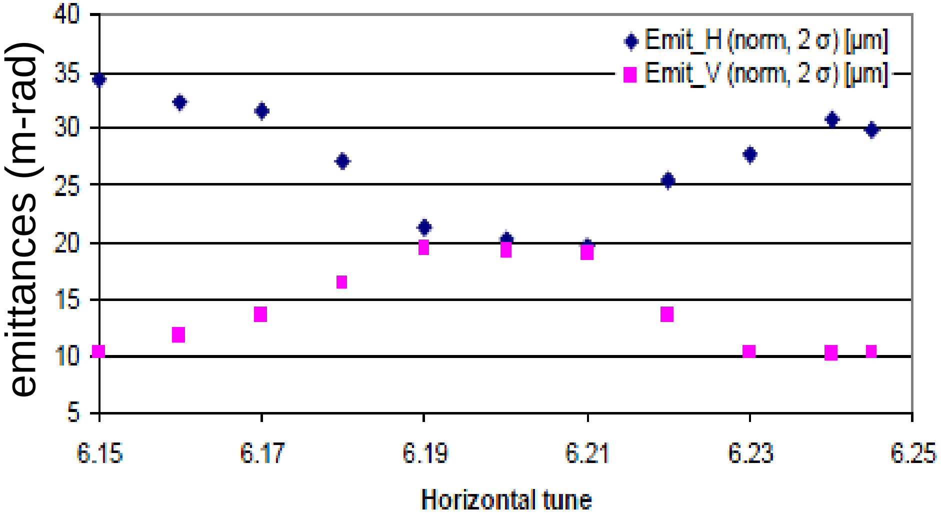

IMPACT simulation

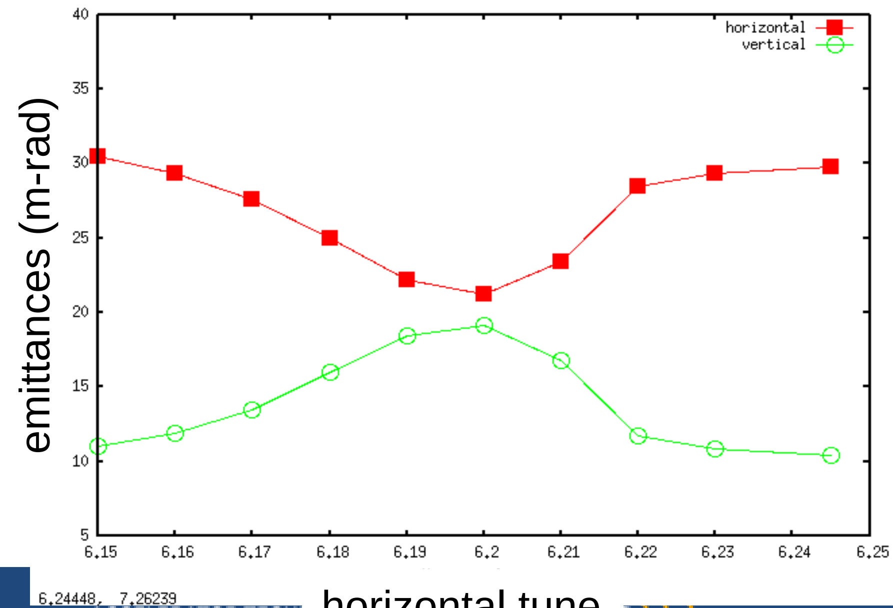

3D IMPACT Simulation Improves Agreement in Dynamic Montague Resonance Crossing at PS

100 ms dynamic Crossing

measurements

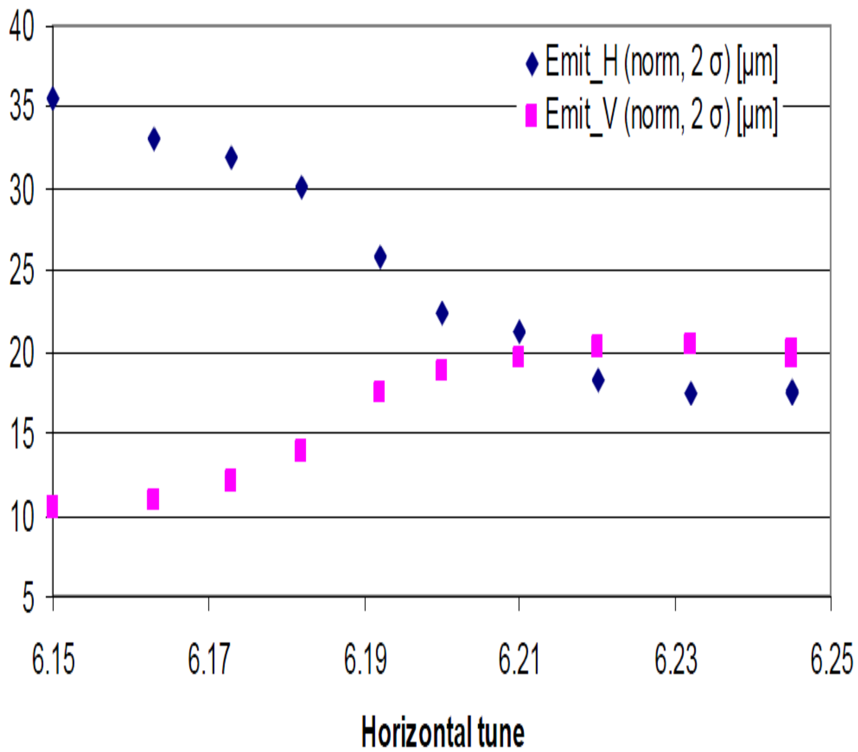

IMPACT simulation:
fully 3D+nonlinear lattice

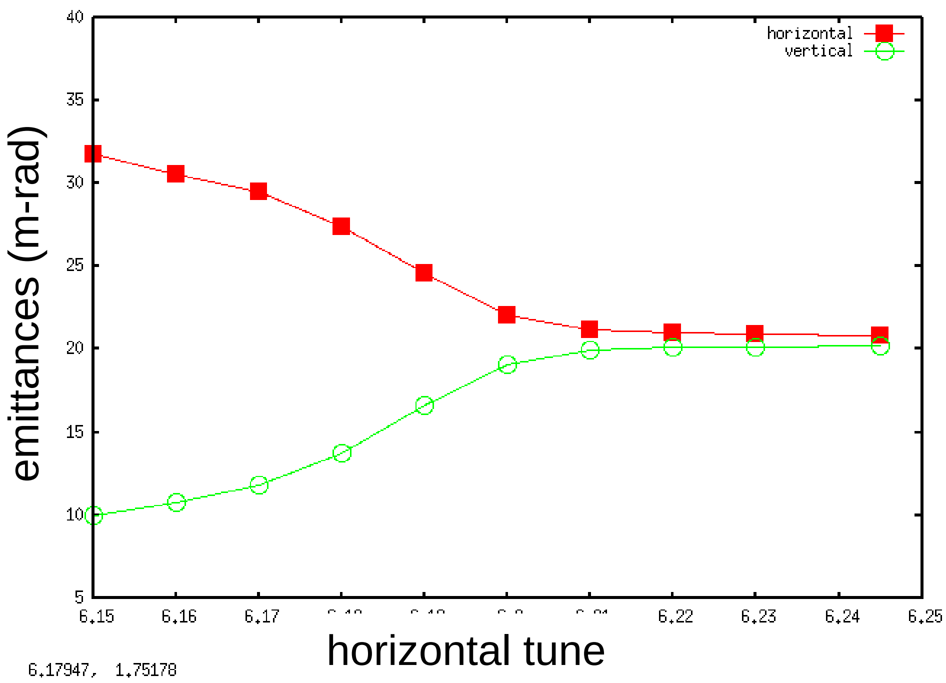

Acknowledgements:

We would like to thank the contributions from all collaborators. This work was supported by the U.S. Department of Energy under Contract No. DE-AC02-05CH11231 and used computer resources at the National Energy Research Scientific Computing Center.

Thank You for Your Attention!